The South China Sea Two Islands Monsoon Experiment for studying convection and subseasonal to seasonal variability

Chung-Hsiung Sui[1, *], Po-Hsiung Lin[1], Wei-Ting Chen[1], Sen Jan[2], Chian-Yi Liu[3], Yiing Jang Yang[2], Ching-Hwang Liu[4], Jau-Ming Chen[5], Ming-Jen Yang[1], Jing-Shan Hong[6], Li-Huan Hsu[7, 8], and Li-Shan Tseng[9]

[1] Department of Atmospheric Sciences, National Taiwan University, Taipei City, Taiwan
[2] Institute of Oceanography, National Taiwan University, Taipei City, Taiwan
[3] Center for Space and Remote Sensing Research, National Central University, Taoyuan City, Taiwan
[4] Department of Atmospheric Sciences, Chinese Culture University, Taipei City, Taiwan
[5] Department of Maritime Information and Technology, National Kaohsiung University of Science and Technology, Kaohsiung City, Taiwan
[6] Central Weather Bureau, Taipei City, Taiwan
[7] Taiwan Typhoon and Flood Research Institute, Taipei City, Taiwan
[8] National Science and Technology Center for Disaster Reduction, Taipei City, Taiwan
[9] Department of Earth Sciences, National Taiwan University, Taipei City, Taiwan

ABSTRACT

The South China Sea (SCS) Two-Island Monsoon Experiment (SCSTIMX) is the observational task of an integrated project aimed to better understand interactions of convection over the SCS and Maritime Continent (MC) with large-scale flow. The project consists of sub-projects in three research groups: convective processes, large-scale dynamics, observations. SCSTIMX is one of the field campaigns of the Years of the Maritime Continent (2017 - 2020). Special observations made or derived for the SCSTIMX are documented in this article that include field campaigns at Taiping and Dongsha islands during intensive observation periods (December 2017, March and May 2018), cruises by the National Taiwan University ocean research vessel (OR1) in December 2016 and December 2017, and satellite observations in the SCS-MC for the project years. We show the spatial-temporal evolution of the La Niña event from December 2016 to June 2018 and embedding interactions of convectively coupled equatorial waves (CCEW) with diurnal cycles and intraseasonal oscillations (ISO) in the SCS-MC. The La Niña-ISO-CCEWs together resulted in the late SCS summer monsoon onset in May 2018. In addition to the La Niña influence, the strong Indian Ocean dipole signal in December 2017 further weakened CCEWs in eastern Indian Ocean. We also show research highlights from participating projects published in the current special issue of TAO.

1. INTRODUCTION

Residing within the Indo-Pacific warm pool, the Maritime Continent (MC) and the South China Sea (SCS) is a water vapor pathway connecting the Indian and East Asian-Western North Pacific monsoon during boreal summer and connecting the most powerful East Asian winter monsoon with the Australian summer monsoon. Because of its special geographic location, convection in the SCS-MC is tightly coupled with the uprising branch of Walker circulation and Hadley circulation. During boreal winter, the SCS encounters the strongest tropical-extratropical interaction and hemispheric interaction (e.g., Chang and Lau 1982; Lau and Chang 1987; Neale and Slingo 2003; Chang et al. 2005). The seasonal march in summer is characterized by onset of convection over Indo-China (April), Bay of Bengal and SCS (May), and followed in August to September by a wide range of variability over Arabian Sea, Northern China, SCS, and WNP (Luo and Yanai 1983; He et al. 1987; Tao et al.

1987; Murakami and Matsumoto 1994; Wang 1994; Wang and Lin 2002).

Within the energetic winter and summer monsoon, the SCS-MC and neighboring Indo-Pacific warm pool have the most prominent intraseasonal (30 - 60 day) and 10 - 20 day oscillations. The 10 - 20 day, or quasi-biweekly, oscillation (QBWO) emerges from the equatorial western Pacific and propagates northwestward with a slight southwest-northeast tilted but mainly longitudinally elongated horizontal structure (e.g., Kikuchi and Wang 2009; Chen and Sui 2010). These features are consistent with the results depicted in other studies (Krishnamurti and Ardanuy 1980; Murakami 1980a, b; Chen and Chen 1995; Fukutomi and Yasunari 1999; Annamalai and Slingo 2001; Hsu 2005; Mao and Chan 2005; Kikuchi and Wang 2009). The QBWO is perceived as a moist equatorial Rossby wave modified by the basic state (Wang and Xie 1998; Chatterjee and Goswami 2004) or a mixed Rossby-Gravity wave (e.g., Goswami and Mathew 1994; Mao and Chan 2005).

Relative to QBWO, intraseasonal oscillations (ISO) are more dominant tropical signals as found by Madden and Julian (1972) and many other studies. The fundamental structure of ISOs, now commonly referred to as the Madden Julian Oscillation (MJO), is understood as convection coupled Kelvin-Rossby mode (e.g., Lau and Peng 1987; Wang and Li 1994; Wang and Chen 2017). Some recent studies showed the MJO is profoundly influenced by the basic moisture field through moisture advection (Maloney 2009; Sobel and Maloney 2012, 2013; Adames and Kim 2016). Furthermore, ISOs in boreal summer (or BSISO) possess more complicated features than the MJO does (Lau and Chan 1986; Nitta 1987; Chen and Murakami 1988; Wang and Rui 1990; Hsu and Weng 2001; Lawrence and Webster 2002; Kikuchi et al. 2012; Lee et al. 2013). These studies showed that BSISOs are generally characterized by eastward propagating cloud clusters from equatorial Indian Ocean to western Pacific with flanking twin cyclonic circulation emanating from the western portion of the leading convective zone. As a result, the OLR anomalies exhibit northwest-southeast tilted structure with pronounced northward propagation over Indian Ocean and western Pacific. The associated dry zone (positive OLR anomalies) also exhibits a similar evolution cycle. Northward propagation has been suggested as a result of barotropic vorticity anomalies in the presence of easterly shear by Jiang et al. (2004) and Drbohlav and Wang (2005). Other mechanisms are also suggested. See DeMott et al. (2013) for a review and an assessment of the various mechanism based on a modeling approach.

It is well known that El Niño-Southern Oscillation (ENSO) powerfully modulates the Pacific Walker Circulation and the MC-SCS precipitation (e.g., Philander 1990; Wang et al. 2000; Wang and Lin 2002). In return, the convection and associated near surface winds in the Maritime Continent and surrounding equatorial Indo-Pacific warm

pool can force equatorial ocean waves to influence ENSO evolution (e.g., Zhang et al. 2018). There are many studies on relevant ENSO dynamic that is beyond the scope of research of this project. We will briefly discuss the rainfall and circulation in the SCS-MC and neighboring oceans in El Niño and La Niña winters later in this article as a climate background of this project.

The monsoon-climate variability discussed above is profoundly influenced by the terrain of the SCS-MC and the resultant diurnal cycle as the most dominant signal relative to intraseasonal, seasonal, and interannual rainfall distribution. The climatological amplitude of the diurnal rain rate shows places of strong diurnal cycle associated with high topography near major islands in the Maritime Continent (Peatman et al. 2014). The strong diurnal heating is crucially linked to the convective variability of longer time scales such as the Madden Julian Oscillation (e.g., Peatman et al. 2014; Sakaeda et al. 2017; Hung and Sui 2018), the monsoon system (e.g., Houze et al. 1981), and ENSO.

The strong diurnal cycle in the MC region has been shown to disrupt the propagation of the Madden-Julian Oscillation through the Maritime Continent (e.g., Hung and Sui 2018; Ling et al. 2019). Model simulations of the MJO are often poor over the region, resulting in local errors in latent heat release and global errors in medium-range weather prediction and climate simulation (Neale and Slingo 2003; Ahn et al. 2020). Therefore, it is important to improve the interaction of convection of with the MJO in models.

Despite the many important roles of the SCS-MC summarized above, progress in understanding and improving weather and climate oscillations in the region is hampered by lack of observations. To overcome the problem, the international project "Years of the Maritime Continent" (YMC) is being organized by Chidong Zhang (University of Miami) and Kunio Yoneyama (JAMSTEC). Scientists from international communities interested in the weather and climate of the MC are invited (including scientists in Taiwan) to work with the MC countries (Indonesia, Malaysia, Singapore, Philippines) to make special observations for the weather-climate system of the MC for 2017 - 2020. Through data sharing, field campaigns, and model assimilations, YMC plans to accomplish the scientific goal: to observe the weather-climate system of the Earth's largest archipelago to improve understanding and prediction of its local variability and global impact.

The SCSTIMX is particularly interested in the enhanced observations of convection and weather and climate oscillations in the SCS-MC region because their influences on Taiwan. In boreal winter, Taiwan is in the direct path of the strong cold surge belt upstream of the Maritime Continent convection systems. Since the cold surge and cold fronts affecting Taiwan are also strongly associated with the intensity and movement of the East Asian jet, any feedback from the tropical convection (e.g., associated with the MJO)

to the midlatitude may also influence the subsequent baroclinic development of weather systems that affect Taiwan (e.g., Jeong et al. 2008; He et al. 2011; Hung et al. 2014).

The outline of the article is as follows. The scientific objectives and special observations of the integrated project are described in section 2. The important climate background for the SCS-MC study is discussed in section 3. The interannual evolution of ocean-atmosphere coupled state during 2016 - 2018 is shown in section 4. In section 5, we show results of influences of ISO and tropical disturbances on Rainfall Variability in the SCS. In section 6, we briefly describe highlights of the project. Finally, relevant web sites and data sets are provided in section 7.

2. THE INTEGRATED PROJECTS AND OBSERVATIONS

Because of the importance of water cycle and convection over the SCS-MC, we proposed an integrated project "Interaction of convection over the SCS-MC with large-scale flow" to study the subseasonal to seasonal climate oscillations and their influences on extended weather and associated rainfall in the SCS-MC. The project was funded for three-year (2016 - 2019) to observe convective and moistening processes and large-scale dynamic processes over the SCS, and to combine the special and all existing observations with models to better understand the convection-dynamics interaction in weather and climate over the SCS and vicinity of multiple time scales ranging from diurnal, synoptic, to intraseasonal and beyond. The integrated project consists of a general project and six sub-projects that can be classified into three research groups. The three groups and their major research themes are shown in Fig. 1. Specific research tasks are described in Table 1.

2.1 Special SCSTIMX Observations

Special observations were made or derived in the SCSTIMX period by the general project and sub-project 5 and 6 (Table 1). Observations were acquired through in situ and remote sensing instruments plus ocean cruises by the NTU research vessel, Ocean Researcher 1 (OR1), in the SCS according to the implementation schedule shown in Fig. 2. The specific atmospheric and ocean observations include the following: surface and vertical profiles of T, q, u, v by radiosondes, wind profilers at Dongsha, Taiping, and OR1; Satellite measurements of cloud properties; Physical oceanography measurements by OR1. See Table 2 for a list of all variables and the corresponding resolutions and periods of the special atmosphere and ocean data. The type of instruments are listed in Table 3.

2.2 Assimilation and Ancillary Data

For sea surface temperature (SST), this study used both NOAA Extended Reconstructed Sea Surface Temperature (ERSST) v5 and NOAA Optimum Interpolation Sea Surface Temperature (OISST) v2. ERSST v5 is a global monthly dataset with spatial resolution 2° latitude × 2° longitude which can be obtained from https://www1.ncdc.noaa.gov/pub/data/cmb/ersst/v5/netcdf/. The dataset is derived from the International Comprehensive Ocean-Atmosphere Dataset (ICOADS) Release 3.0 SST, which comes from Argo floats above 5 m, Hadley Centre Ice-SST version 2 (HadISST2) ice concentration (Huang et al. 2017). OISST is an analysis merging observations from platforms such as satellites, ships, and buoys (Banzon et al. 2016). The OISST data set used in this study is derived from Advanced Very High Resolution Radiometer (AVHRR) with 0.25° and daily resolution. Data period from 1981 to 2018 for both datasets is used in this study.

Meteorological data used in this study is the European Centre for Medium-Range Weather Forecasts Reanalysis Interim (ER-Interim) that is produced by the integrated forecast system IFS-Cy31r2, 2006 release (Berrisford et al. 2011). The data resolution is 0.75° latitude × 0.75° longitude and 60 vertical levels from the surface up to 0.1 hPa. The data is available from the website of the ECMWF (https://www.ecmwf.int/en/forecasts/datasets/archive-datasets/reanalysis-datasets/era-interim). January 1979 to December 2018 was applied to our analysis.

Two precipitation data set are analyzed. One is the Climate Prediction Center (CPC) morphing technique (CMORPH), V1.0. In this version, the purely satellite-based CMORPH precipitation estimates are reprocessed and bias corrected against the CPC daily gauge analysis over land and the GPCP pentad merged analysis of precipitation over ocean (Joyce et al. 2004; Xie et al. 2017). The data period of CMORPH precipitation we used in this study is from 1998 to 2018 and the spatial resolution is 0.25° latitude × 0.25° longitude. It can be accessed from ftp://ftp.cpc.ncep.noaa.gov/precip/CMORPH_V1.0/. The other precipitation data is the Global Precipitation Climatology Project (GPCP) Monthly Precipitation Analysis, Version 2 (Adler et al. 2003). GPCP produces a consistent analysis of global precipitation from an integration of various satellite data sets over land and ocean and a gauge analysis over land. Spatial resolution is 2.5° and period from 1979 to 2018 was used.

We analyzed sea level pressure from the NCEP Reanalysis, Version 1. The dataset involves the recovery of land surface, ship, rawinsonde, pibal, aircraft, satellite, and other data; quality controlling and assimilating these data with a data assimilation system that is kept unchanged over the reanalysis period (Kalnay et al. 1996). The data analyzed has a horizontal resolution of 2.5° latitude × 2.5° longitude for the period of 1981 to 2018 is applied.

We also used Outgoing longwave radiation (OLR) as an appropriate proxy for the convection, which is based on the interpolated daily OLR version 1.2 from National Oceanic

and Atmospheric Administration (NOAA) Climate Record (CDR). The data can be downloaded from the website of NCEI (National Centers for Environmental Information), NOAA (https://www.ncei.noaa.gov/data/outgoing-long-wave-radiation-daily/access/). It is estimated from High-Resolution Infrared Radiation Sounder (HIRS) radiance observation with a two-day lag. Spatial resolution is 1° latitude × 1° longitude (Lee and NOAA CDR Program 2011).

Niño 3.4 SST anomaly and Southern Oscillation Index (SOI) from NOAA's Climate Prediction Center (https://www.cpc.ncep.noaa.gov/data/indices/) were used to indicate the phase of ENSO. Niño 3.4 SST anomaly is derived from ERSST v5 with climatology period 1981 - 2010. The detail method of SOI calculation is in the website of CPC (https://www.cpc.ncep.noaa.gov/data/indices/Readme.index.shtml).

3. SCIENTIFIC BACKGROUND AND QUESTIONS

The climatological monsoon and rainfall in the SCS-MC and neighboring warm pool in boreal winter and summer is shown by the monthly mean fields of rain intensity, SST, and 925 hPa wind from November to June in Fig. 3. In November and December, the warm pool in southwestern Pacific and Arafura Sea is broader and warmer (SST > 29.5°C) than the warm SST in tropical Indian Ocean. The western Pacific warm pool then weakens while the Indian Ocean warm pool strengthens from January to March. By April and May, SST in northern tropical Indian Ocean
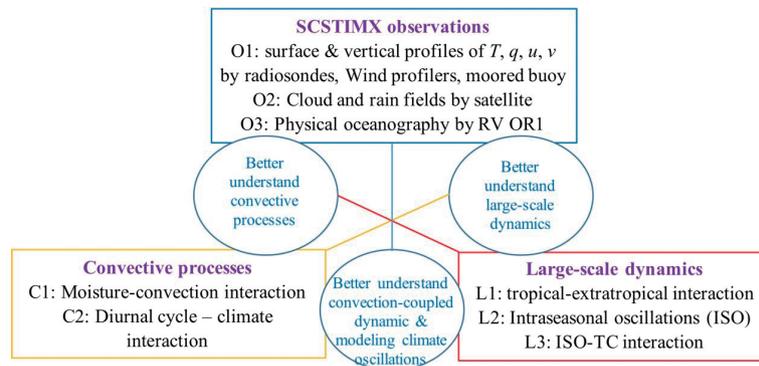

Fig. 1. Research areas and the SCSTIMX observations of the integrated project "Interaction of convection over the MC-SCS with large-scale flow" summarized in three groups and their mutual links that demand integrated research for improving understanding/prediction of subseasonal to seasonal scale variability.

Table 1. List of research tasks (sub-projects). Affiliations of PIs and Co-PIs include National Taiwan University (NTU), National Central University (NCU), National Taiwan Normal University (NTNU), National Kaohsiung Marine University (NKMU), Chinese Culture University (PCCU), Central Weather Bureau (CWB), Taiwan Typhoon and Flood Research Institute (TTFRI), and Taiwan Ocean Research Institute (TORI).

| Project	PI and Co-PIs (Affiliation)	Project Title
General Project	Chung-Hsiung Sui (NTU) Po-Hsiung Lin (NTU) Yu-Chieng Liou (TTFRI) Yih Yang (TORI) Pay-Liam Lin (NCU) Ching-Hwang Liu (PCCU)	Observation of convection and multiscale oscillations in the SCS-MC climate system
Sub-project 1	Chung-Hsiung Sui (NTU) Ching-Hwang Liu (PCCU) Li-Shan Tseng (NTNU)	Boreal summer intraseasonal variability and winter midlatitude-tropical interactions over the South China Sea and vicinity
Sub-project 2	Jau-Ming Chen (NKMU)	ISO-TC Interactions in the SCS-MC
Sub-project 3	Ming-Jen Yang (NTU) Jing-Shan Hong (CWB)	The Interaction between Moisture Transport and Convection over the South China Sea and Maritime Continent
Sub-project 4	Wei-Ting Chen (NTU) Chien-Ming Wu (NTU)	Diurnal Variations of Moist Processes over the South China Sea and Their Representation in Global Models
Sub-project 5	Chian-Yi Liu (NCU) Wei-Ting Chen (NTU)	Next generation satellite observations of SCS Convection Processes
Sub-project 6	Sen Jan (NTU) Chung-Hsiung Sui (NTU) Yiing Jang Yang (NTU) Ming-Hui Chang (NTU)	Air-Sea Interaction in the South China Sea and its connectivity with Maritime Continent
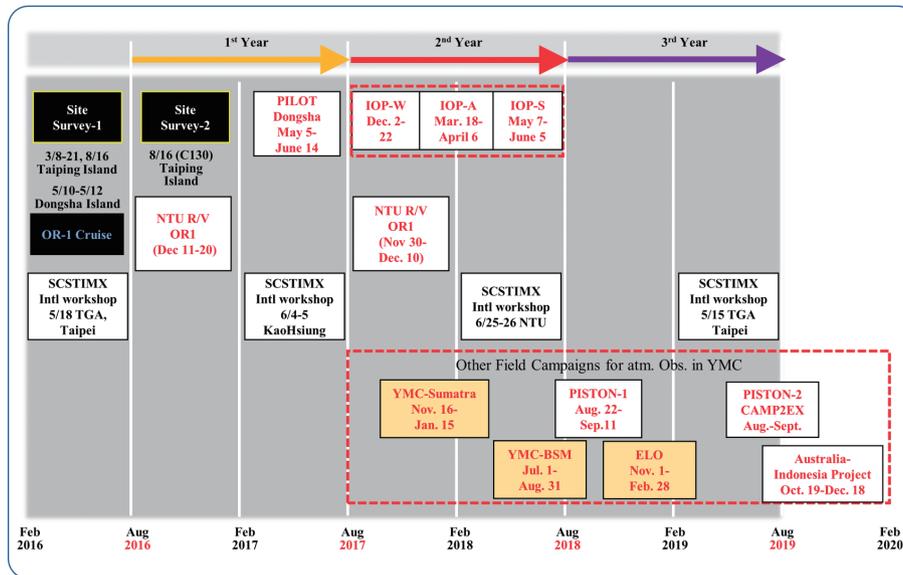
Fig. 2. Implementation schedules for the SCSTIMX that are carried out by the integrated project "Interaction of convection over the SCS-MC with large-scale flow" (August 2016 to July 2019). Special SCSTIMX observations were made during one pilot phase, three IOPs (IOP-W, IOP-A, IOP-S), and two NTU R/V OR1 cruises. Also shown are schedules of annual SCSTIMX workshops and other YMC field campaigns.

Table 2. Special atmosphere/ocean data observed /derived for SCSTIMX.

Radiosonde [H, P, T, RH, WS, WD]	
Dongsha regular measurements	2009/9 - current, [once per day]
SCSTIMX (Dongsha)	PILOT (2017/5/05 - 6/14), IOP-A (2018/3/18 - 4/06), [2 - 4 times per day]
SCSTIMX (Dongsha, Taiping)	IOP-W (2017/12/02 - 12/22), IOP-S (2018/5/07 - 6/05), [2 - 4 times per day]
NTU R/V OR1	2016/12/11 - 12/22, 2017/11/30 - 12/10, [1 - 4 times per day]
PISTON-1 (Dongsha, Taiping)	2018/8/22 - 9/11 [4 times per day]
Surface observation at Dongsha (D) and Taiping (T)	
Wind profiler [u, v, w], vertical res: 50 m < 3 km, ~100 m within 3 - 9 km, ~200 m > 9 km	2017/6 - 12 (D); 2018/4/16 - 6/03 (T), [10 min]
Radiometer [RH, T] vertical res: ~50 m < 0.5 km, ~100 m within 0.5 - 2 km, ~100 m within 2 - 10 km	2017/5/14 - 6/14 (D); 2017/6 - 12 (D); 2017/12/03 - 12/09 (T); 2018/4/16 - 6/03 (T), [~2 min]
Weather station [P, T, RH, Rain, WD, WS]	2017/5/05 - 6/14 (D); 2017/12/04 - 2019/3/02 (T), [1 min]
Ceilometers [cloud base height]	2017/5/6 - 6/14 (T); 2017/12/3 - 2018/6.3 (T), [5 s]
Fisheye lens [cloud cover]	2018/1/29 - 2/27; 2018/4/15 - 4/29
Aerosol Lidar	2018/3/18 - 4/06 (D)
Satellite: Himawari-8 Advanced Himawari Imager (AHI)	
Cloud Product [cloud top temp., pre. and height; phase, type, mask, optical thickness, droplet effective radius, liquid and ice water path]	2017/2 - 2018/1 2018/2 - 2019/1 (to be completed) [30 min], [10°S - 30°N; 105°E - 130°E]
Brightness temperature in 3.89, 6.24, 6.94, 7.35, 8.59, 9.64, 10.41, 11.24, 12.38, 13.28 microns	2017/2 - 2018/1 (5 months completed) 2018/2 - 2019/1 (to be completed) [30 min], [10°S - 30°N; 105°E - 130°E]

Table 3. Instruments.

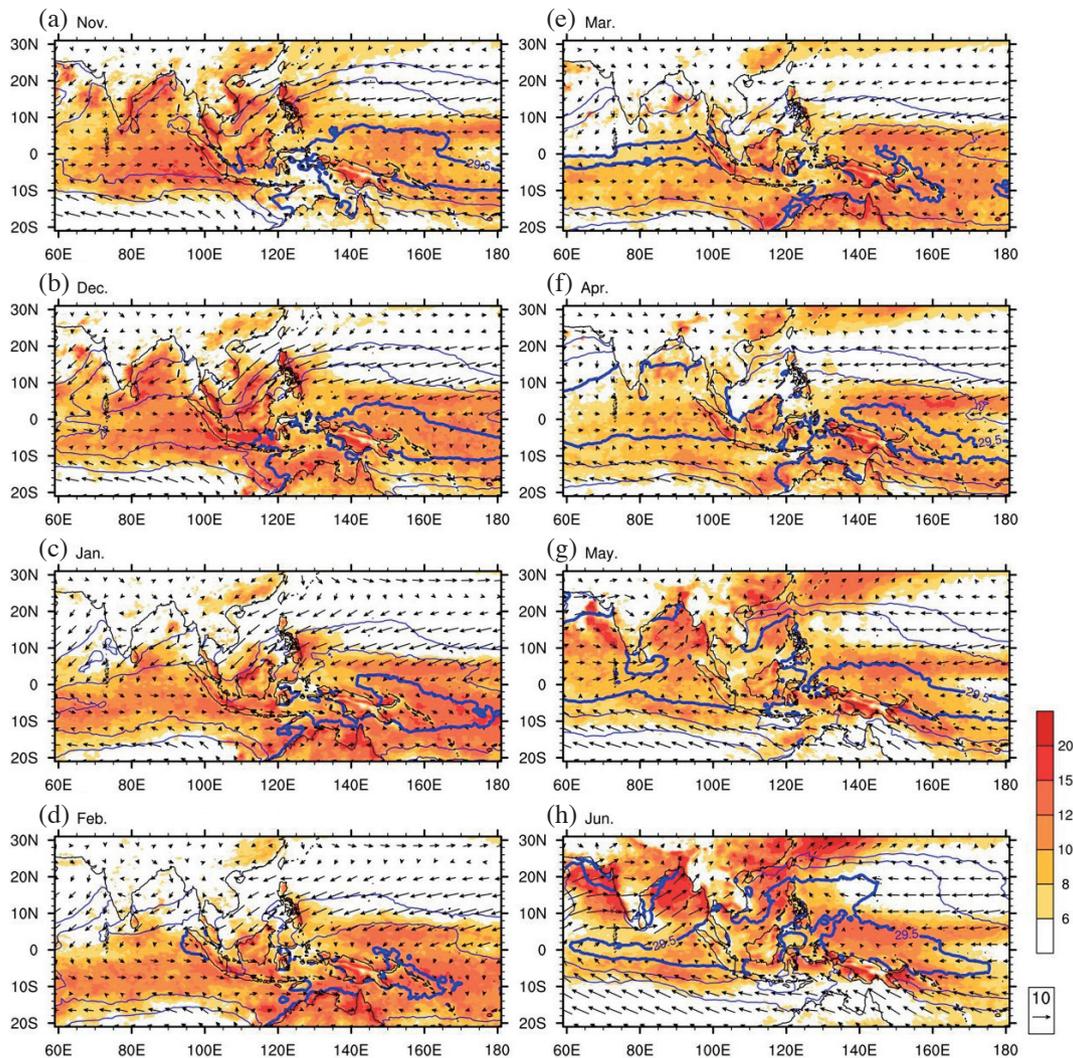|	**Manufacturer**	**Model**
Radiosonde	Vaisala	RS41
Wind profiler	Raptor	FBS-ST (D), XBS-BL (T)
Radiometer	Radiometrics	MP-3000A
Weather station	Vaisala	WXT520
Ceilometer	Vaisala	CL31
Fisheye lens	CMS Schreder	ASI-16

Fig. 3. Monthly climatological (1998 - 2016) maps of precipitation intensity (total rainfall divided by rainy days; shaded; mm day^{-1}), 925-hPa horizontal wind (vectors; m s^{-1}), and SST (blue contours; °C) for (a) - (d) winter months (November, December, January, February) and (e) - (h) spring months (March, April, May, June), where thick contours denote 29.5°C SST isotherms and thin ones denote 27.5 and 28.5°C.

becomes warmer (SST > 29.5°C) and broader than the western Pacific warm pool. The rainfall exhibits a seasonal movement of the Inter-Tropical Convergence Zone (ITCZ) from central and eastern Indian Ocean in November to the Maritime Continent and southwest Pacific (the South Pacific Convergence Zone, SPCZ) in February. From spring in March and April to early summer in May and June, the Indian Ocean ITZC and SPCZ weakens but boreal summer monsoon rain develops rather rapidly in northern tropical oceans (eastern Arabia Sea, Bay of Bengal, SCS). Associated with the seasonal rainfall changes, the low-tropospheric circulation exhibits a clear reversal from winter to summer monsoon in Asian-Australian region

Figure 3 also shows dominant mesoscale terrain-induced rainfall features in the northeasterly monsoon regime beyond 5°N such as east of the Philippines and Vietnam, eastern coast of Malay Peninsula, and north of Sumatra, northeast and northwest of Borneo in the South China Sea that migrates southward from November to January as point-

ed out by Chang et al. (2005). Chang et al. (2005) also pointed out an asymmetry in the degree of intrusion of the boreal winter regime extends northward into the boreal summer regime, whereas the southward extension of the boreal summer regime south of the equator is relatively limited. The asymmetry features are attributed by Chang et al. (2005) to stronger baroclinicity over the cold Asian continent during boreal winter and few coastal areas between 5 - 10°S.

3.1 Monsoon Rainfall Interannual Variability in the Maritime Continent

While ENSO is known to directly influence Maritime Continent precipitation through the Pacific Walker Circulation, the correlation between them in the wet season (boreal winter) is weak, while that in dry season is significantly negative (e.g., Ropelewski and Halpert 1987). This is consistent with composite fields of rainfall and 850hPa wind for the La Niña and El Niño winters (Fig. 4) that show rainfall
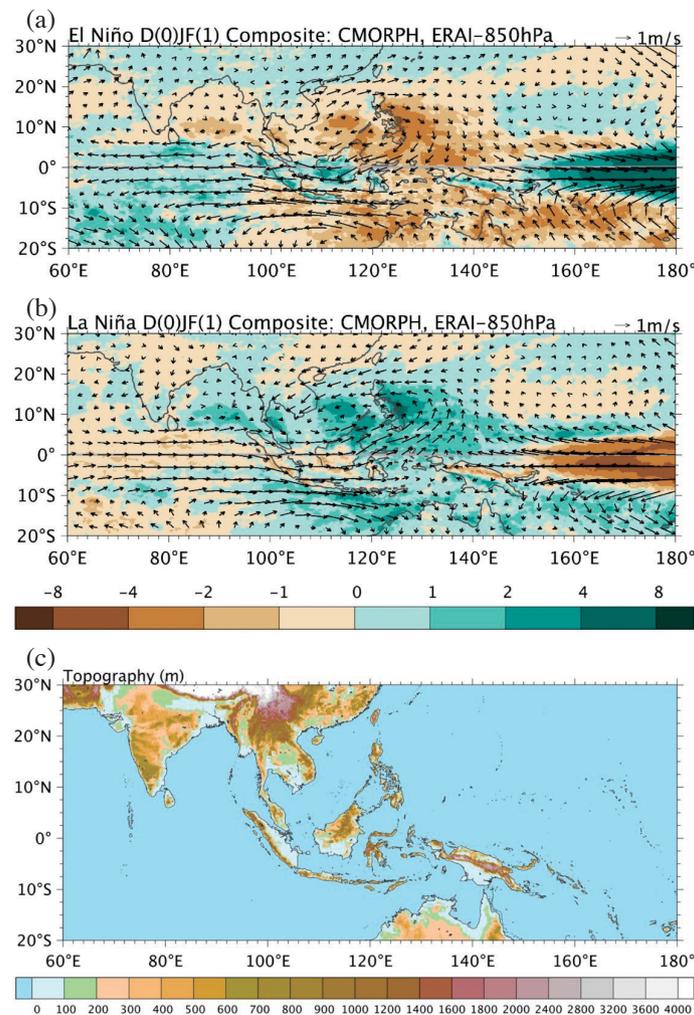

Fig. 4. Composite fields of ERA-Interim 850-hPa wind (vectors) and CMORPH precipitation anomalies (shading; mm day^{-1}) in the mature winter (DJF) of (a) El Niño and (b) La Niña based on 1998 - 2016 monthly climatology. (c) The terrain height (m) from ETOPO5. The El Niño (La Niña) events are 2002/03, 2004/05, 2006/07, 2009/10, 2014/15 (1999/2000, 2000/01, 2005/06, 2007/08, 2008/09, 2010/11, 2011/12, 2016/17, 2017/18).

anomalies over the major islands in the Maritime Continent are of opposite sign with that of surrounding oceans. The low correlation during boreal winter have been studied by Haylock and McBride (2001), Hamada et al. (2002), Hendon (2003), Zhang et al. (2016a, b), and Jiang and Li (2018). Chang et al. (2004, 2016, 2017) suggested that the key reason of the low ENSO correlation with boreal winter rainfall is related to the interaction between the anomalous circulation and the complex terrain in the region (Fig. 4c). The anomalous circulation includes the equatorial zonal flow and the subtropical anticyclonic (cyclonic) flow over the Indo-Pacific warm pool forced by anomalous heating (cooling) associated with El Niño (La Niña) that peak in winter (Jiang and Li 2018). The lack of correlation between MC rainfall and ENSO in boreal winter appears to be related to the low skill in seasonal prediction of MC rainfall in major climate prediction models (e.g., Zhang et al. 2016a, b).

Besides ENSO, the Indian Ocean dipole can also influence rainfall over the Maritime Continent and the SCS. The Indian Ocean dipole (IOD) is characterized by negative SSTA over the eastern tropical Indian Ocean (TIO) and positive SSTA over the western TIO (Saji et al. 1999; Yamagata et al. 2004). Some studies suggested that the IOD is remotely forced by an El Niño event through easterly anomalies over the equatorial Indian Ocean or a reversed process in a La Niña event (e.g., Li et al. 2003; Fan et al. 2017; Feng and Duan 2018). The IOD may influence the atmospheric circulation anomaly over TIO (Li et al. 2003), the Asian monsoon region (e.g., Xu et al. 2016), and tropical Pacific Ocean (e.g., Kug et al. 2006; Luo et al. 2010; Izumo et al. 2014).

The above discussions provide a climatological background for answering the following challenging question:
• How to improve seasonal simulation and prediction in the Maritime Continent?

3.2 The MJO/BSISO/Monsoon and Diurnal Cycle

Although many studies have discussed the role of moisture, radiation, and surface turbulent fluxes to the development and propagation of the MJO, most of them focus on the Indian Ocean region, where the MJO initiates and propagates eastward, within a relatively short period. Yet, the eastward propagation is not a smooth path, with the strength of convective activities changing substantially from locations. For a typical life cycle of the MJO, the convective envelopes initiate from the western Indian Ocean, strengthen over the center Indian Ocean, detour southward (northward) in boreal winter (summer) while passing through the Maritime Continent, re-intensify upon reaching the west Pacific, and finally dissipate around date line. Thus, the complex topography and land-sea contrast over the Maritime Continent and the South China Sea strongly modulate the MJO evolution. Studies have shown that the influence of MC on

the MJO is through very active diurnal cycle of convection that is profoundly modulated by the MJO (e.g., Qian 2008; Oh et al. 2012; Peatman et al. 2014).

Hung and Sui (2018) analyzed diurnal convection and the MJO in the MC region. For the suppressed (convective) stage of the MJO in the Maritime Continent (central Indian Ocean), their composite fields (Fig. 5, left panels) show anomalous easterlies, subsidence and enhanced diurnal convection in the MC. Unlike the low-level wave convergence and advective moistening in IO that both occur in the equatorial zone, advective moistening in the MC occurs primarily south of equator causing a southward detour of the eastward-propagating MJO. Hung and Sui (2018) suggested that this is due to a strong diurnal mixing over the large islands in MC causing more humid boundary layer than that of surrounding oceans that is modulated by equatorial convergence in the lower troposphere associated with the MJO (Kevin wave). Advection of moisture by intraseasonal zonal winds causes drying at windward side and moistening at lee side (Fig. 5, bottom left panel). The inhomogeneous moisture advection and dampened zonal winds in lower troposphere by more active diurnal mixing tends to disrupt eastward propagation of intraseasonal oscillations. A reversed circulation, rainfall, and diurnal rainfall amplitude in MC appear in the opposite phase of the MJO (Fig. 5, right panels). A similar composite performed for the boreal summer intraseasonal oscillations (BSISO) is shown in Fig. 6. The features of the composite wind/convection and diurnal cycle in the equatorial zone within the MC for the BSISO appears the same as that for the MJO but the major BSISO convection/circulation center is shifted northward to the SCS in Fig. 6.

Observational studies of modulation of diurnal cycle by the MJO in the Maritime Continent suggest a strong interaction between the two scales of oscillations. Modeling studies of the MJO and diurnal cycle indicate a close link of the diurnal cycle and the MJO that is further related to the mean state of the simulated climate (e.g., Oh et al. 2013; Peatman et al. 2015). These studies along with other modeling studies show the important role of the Maritime Continent in global climate that is a major scientific motivation for the YMC project.

The onset of the SCS summer monsoon (SCSSM) is considered a precursor of the East Asia summer monsoon (EASM) onset (Tao et al. 1987; Tanaka 1992; Lau and Yang 1997). The onset and evolution of EASM is closely related to the northward propagation of the climatological intraseasonal oscillation (CISO) (Nakazawa 1992; Wang and Xu 1997; Kang et al. 1999) or the "fast" annual cycle (Lin and Wang 2002). It only takes 5 days or so for the rain band to quickly expand and establish over subtropical Pacific (Wang and Lin 2002), and active cross-scale interactions of convection are involved. Two recent works have investigated the role of the land diurnal cycle and coastal organized convection during the fast transition of SCSSM onset.
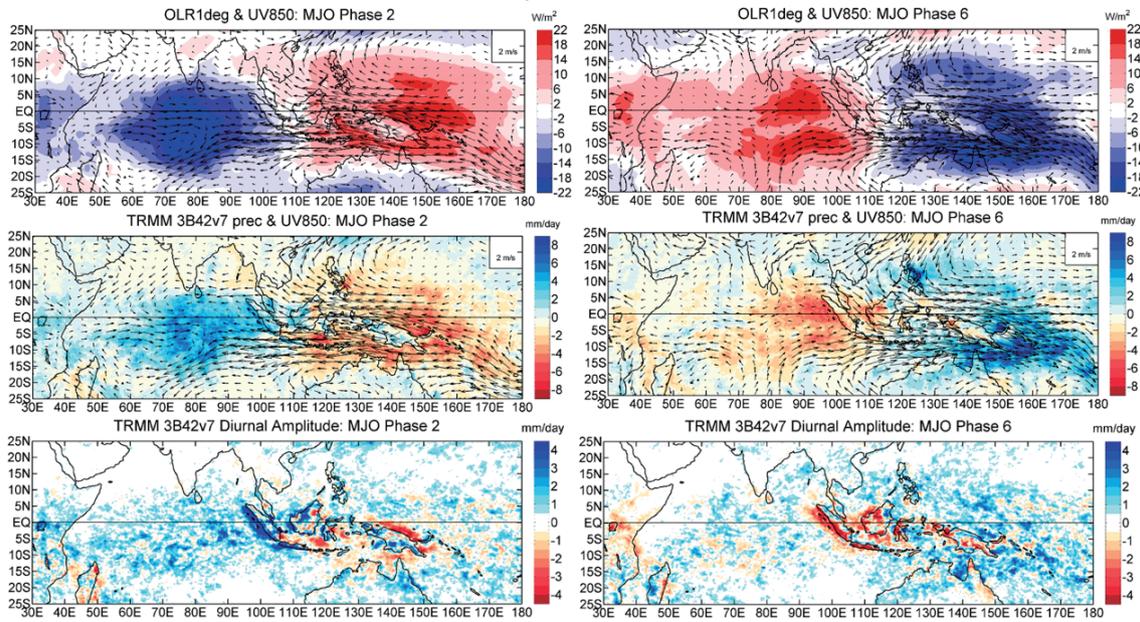
MJO composite (all events)

Fig. 5. The 20-60-day filtered OLR (shading in top panels; W m^{-2}), 850-hPa winds (vectors in top and middle panels; m s^{-1}), rainfall amount (shading in middle panels; mm day^{-1}), and diurnal rainfall amplitude (shading in the bottom panels), composited for the MJO phase in boreal winter when Central Indian Ocean is convective while the Maritime Continent is suppressed (phase 2, left panels) and for the opposite phase of the MJO (phase 6, right panels). See Hung and Sui (2018) for details.
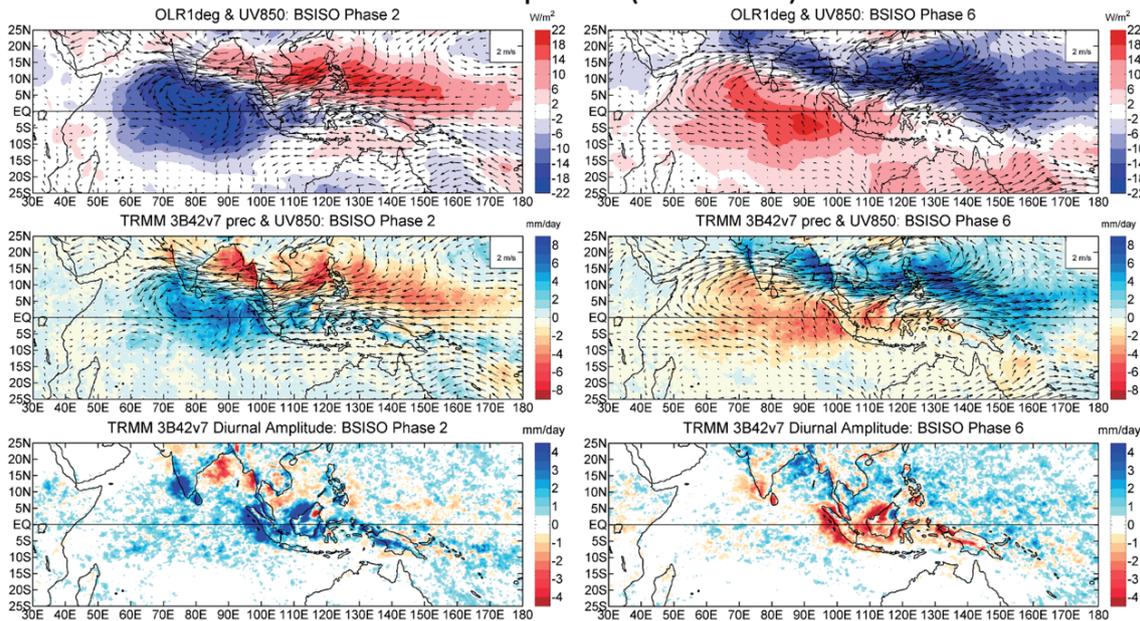
BSISO composite (all events)

Fig. 6. As in Fig. 5 but for boreal summer intraseasonal oscillations.

Using climatological statistics of satellite observations and idealized cloud-resolving simulations, Chen et al. (2019a) identified that, during the pre-onset period, the prominent diurnal cycle over the land areas surrounding the SCS is associated with a basin-scale (~1000 km) local circulation. The anomalous subsidence of this circulation is a key factor suppressing the convection over the ocean, while the diurnally triggered coastal convection is less organized and confined near the coastal ocean. During the onset pentad, the low-level westerly provides a vertical shear structure that facilitates the development of large (> 300 km), propagating coastal convective systems. With the number of these organized systems increases prominently and penetrates further from the coast into the open ocean, they significantly contribute to the sharp moisture buildup over the ocean within 10 days after onset. On the other hand, Chen et al. (2019b) investigated the systematic bias of precipitation during the SCSSM onset period contributed by the interactions among the fast physical processes in a global climate model using a multi-year hindcast (a.k.a TransposeAMIP) approach. The model underestimates the pre-onset basin-scale local circulation and the post-onset coastal organized convection, both can be associated with the overall weaker EASM rainfall. These biases during the SCSSM onset period were further linked to the unrealistic representation of the timing and the amplitude of the diurnal cycle, as well as the precipitation-moisture sensitivity by the physics parameterizations.

The above results raise two challenging questions for further research:

• How does the convective-radiative heating distribution (horizontal, vertical and temporal structure) affect the propagation and growth of the MJO and BSISO?
• How does the evolution of monsoon, the MJO (BSISO) and diurnal convection in the Maritime Continent (South China Sea) mutually influence each other?

4. LARGE-SCALE BACKGROUND OF 2016 - 2018 IN THE LA NIÑA CONDITION

The SCSTIMX observations were carried out during December 2017 and June 2018. The period was mostly in the La Niña phase following the 2014 - 2016 prolonged ENSO. The evolution is shown by Niño 3.4 and Southern Oscillation Index (Fig. 7), and Hovmoller diagram of SST, OLR, and 850-hPa zonal wind at equator (Fig. 8). The prolonged ENSO event evolved in the following sequences: La Niña phase in D(-1)JF(2014), weak El Niño in D(-1)JF(2015), IOD in SON(2015), primary El Niño D(-1)JF(2016), and a fast decay to La Niña by JJA2016. Following summer of 2016, a weak La Niña condition developed, and the Niño 3.4 reached a minimum in December 2016, while the SSTA over tropical western Pacific and eastern Indian Ocean was warm (Figs. 7, 8a). The cold SSTA and easterly anomalies associated with the La Niña condition in the period acted to

recharge the equatorial heat content (warm water volume) that tend to lead to a phase transition. Indeed, the strong and persistent SST-wind coupling in 2017/2018 (Figs. 8a, b) led to the development of a weak warm winter in December 2018 (Fig. 7).

The climate condition for the field campaigns in the pilot study (December 2016) and SCSIMX-W (December 2017) is shown by the seasonal anomalous fields of SST/SLP, and 850 hPa stream function/rain from winter 2016/17 to 2017/18 (Fig. 9). In D(-1)JF(2017), the rainfall was suppressed in central equatorial Pacific, Indian Ocean, western Maritime Continent, and enhanced over neighboring regions including the SCS, Philippine Sea, eastern Maritime Continent, Timor Sea, Arafura Sea, northern Australia, Pacific ITCZ and SPCZ (Fig. 9b). The tropical circulation coupled with equatorial cooling/heating consisted of a pair of off-equatorial anomalous cyclonic circulation along the longitude band centered at 100°E. The northern cyclone/heating over Indo-China Peninsula induced southwesterly into the South China Sea. The southern cyclone/heating south of MC together with suppressed precipitation and the anticyclonic circulation anomaly over southern Indian Ocean resulted in the cold SSTA over southern Indian Ocean through wind-evaporation-SST feedback (Fig. 9a). The cooler equatorial SST in the boreal winter was accompanied with weakened Aleutian Low and northward shifted westerly jet over North Pacific. Cold (warm) SSTA below (in the southern flank of) the weakened Aleutian Low may be a result of wind-evaporation-SST feedback. The overall anomalous fields of SST, wind, and diabatic heating weakened in MAM2017 (Figs. 9c, d) and the cold SSTA in equatorial Pacific disappeared. This is likely due to seasonally weaker SST gradient and trade wind in spring and consequently weaker ocean-atmosphere coupling strength in equatorial Pacific. But the anomalous anticyclonic flow over northeastern Pacific strengthened and extended southwestward to western subtropical Pacific.

Following the annual cycle of cold tongue that is weakest in spring and strongest in fall, cold SSTA emerged again in equatorial eastern Pacific in summer (JJA2017) and grew through fall to the coldest stage in D(-1)JF2018. The above development of La Niña in equatorial Pacific was coupled with strengthening easterly and dry anomalies in central and eastern Pacific while convection in western Pacific largely remained enhanced. The extratropical circulation exhibited contrasting features in boreal summer and winter monsoon regimes. In the summer monsoon regime (JJA2017), Fig. 9f shows a train of wave packets extending from the Maritime Continent, across subtropical western north Pacific, Japan, North Pacific, to North America. A corresponding atmospheric heating and cooling anomalies were located over the Maritime Continent and subtropical western North Pacific, respectively. In SON2017 and D(-1)JF2018, the colder SSTA over Niño 3.4 region than that of D(-1)JF2017
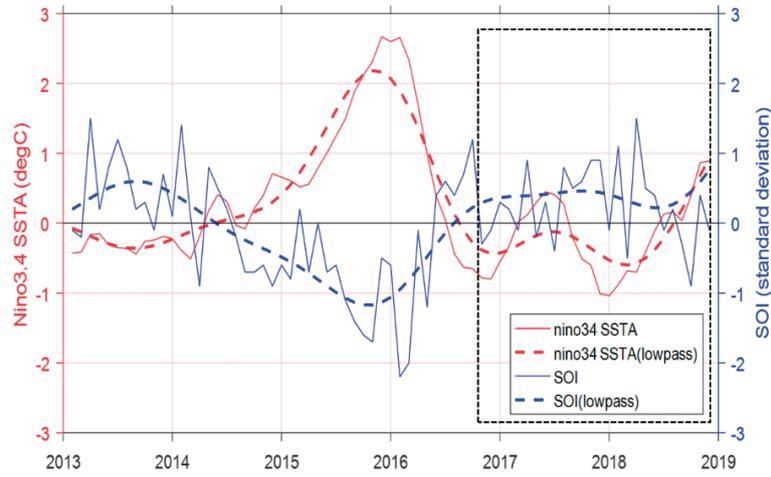
Fig. 7. Monthly evolution of Niño 3.4 SST anomaly (red) and normalized Southern Oscillation Index (SOI; blue). The dashed lines are Butterworth low-pass filtered SST and SOI (cutoff frequency = 1/year).
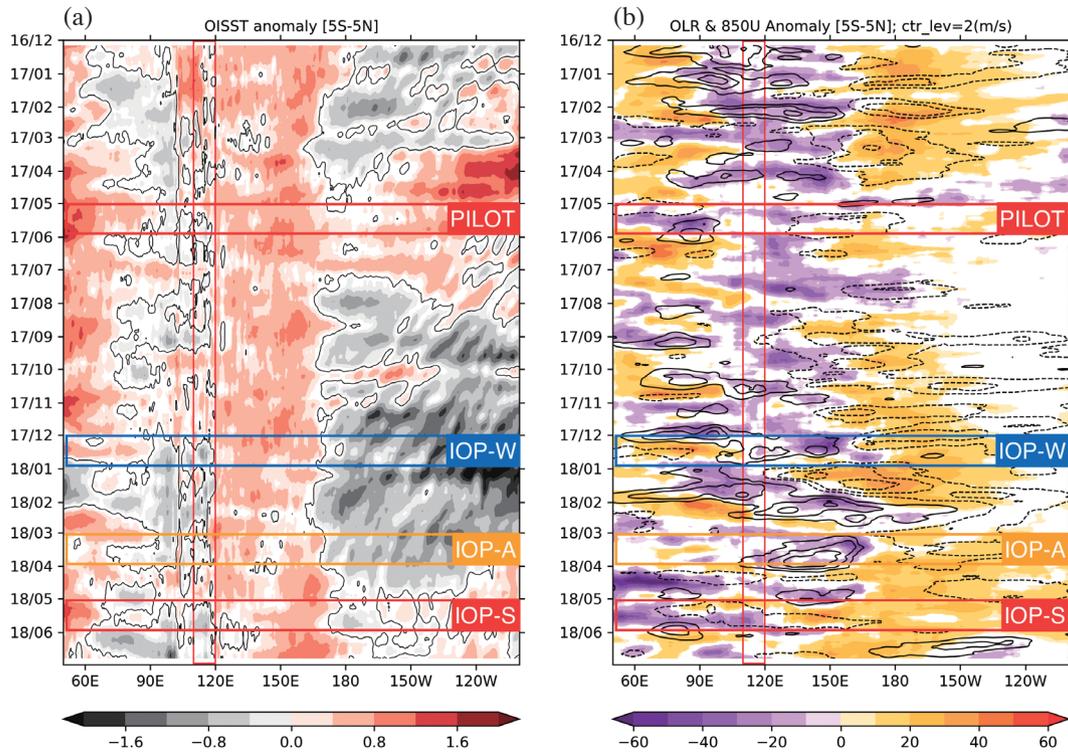

Fig. 8. Hovmöller diagram for equatorial (5°S - 5°N) (a) OISST (°C) (b) OLR (shading; W m^{-2}), and zonal wind (contour) anomalies based on the 1980 - 2017 climatology of long-term average and the first-three annual harmonics. A 11-day moving average is applied to all variables. The black contour in (a) denotes the zero-value line for OISST anomaly. The Solid (dashed) contours in (b) are westerlies (easterlies) with the interval of 2 m s^{-1}, and the zero-value contours are omitted. The longitudinal band of 110 - 120°E and the four IOPs for the SCSTIMX are marked.
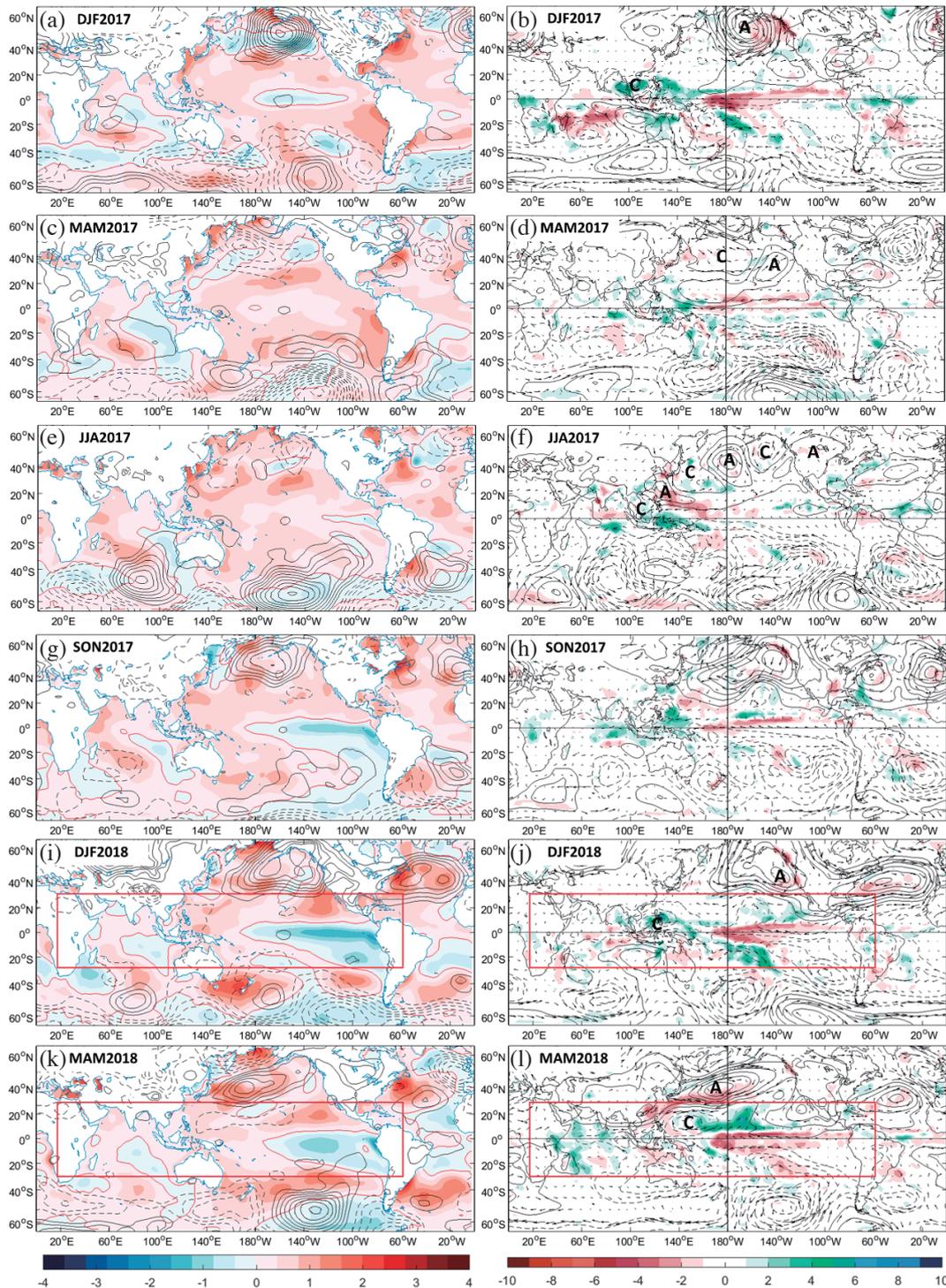
Fig. 9. Left panels: anomalous fields of ERSSTv5 (shading), and NCEP-R1 SLP (contoured at 1-hPa intervals); right panels: GPCP rainfall (shading), ERA-Interim 850-hPa stream function (contour at 10^6 m^2 s^{-1} intervals) and ERA-Interim 850-hPa winds for six consecutive seasons from D(-1) JF2017 to MAM2018. The anomalies are based on 1981 - 2010 monthly climatology. Solid (dashed) contours denote positive (negative) values and the zero-value contours are omitted. The characters "A" ("C") indicate the center of anti-cyclonic (cyclonic) circulation anomalies.

resulted in a weaker Aleutian Low again (Figs. 9h, j). The anomalous cold tongue featured stronger meridional gradient, cross-equatorial southerlies and northward displaced ITCZ, symbolizing the development of Pacific Meridional Mode (PMM; Chiang and Vimont 2004).

From winter to spring 2018 (Figs. 9k, l), the overall La Niña features generally remained but the warm SST and wind associated with the PMM and the anomalous anticyclonic circulation over north Pacific persisted and moved southwestward to western Pacific near 140°E where an anomalous cyclonic circulation and enhanced convection appeared east of Philippine Sea. The enhanced convection over equatorial and northern Indian Ocean in Fig. 9l was a result of two intraseasonal oscillations formed in April and May respectively. The tropical diabatic heating over Indian Ocean and western Pacific together maintained an anomalous anticyclonic circulation over the SCS and Bay of Bengal. See Lu et al. (2020) for more discussions.

5. INFLUENCES OF ISOS AND TROPICAL DISTURBANCES ON RAINFALL VARIABILITY IN THE SCS-MC DURING THE SCSTIMX (2016 - 2018)

The analysis of climate background in the previous section indicates that winter 2016/17 and 2017/18 were in La Niña condition. In this section, we show intraseasonal variability, convective coupled equatorial waves (CCEW), and their modulation of rainfall. Tsai et al. (2020) analyzed the MJO, CCEW and subseasonal peak rainfall in the SCS-MC region. The CCEWs include Kelvin waves (KW), equatorial Rossby waves (ER) and mixed Rossby gravity and TD-type disturbances (MT). The subseasonal peak rainfall is defined as the highest 15-day accumulated rainfall during NDJF within $10°$ latitude $\times$ $10°$ longitude grids. An analysis based on 20 years of data (1998 - 2018) showed the extreme events are strongly modulated by the MJO (occurrence time) and the MT and ER waves (intensity). For the winter of 2017/18 (SCSTIMX-W), the event was modulated by ER north of 5°N and by the MJO on the timing of western Borneo peak events south of 5°N.

Chen et al. (2019c) analyzed intraseasonal variability, CCEW, and rainfall in December 2016. The analysis revealed a dominant ER wave (or 10 - 20 day oscillation) and three KWs interacting with synoptic disturbances, diurnal cycle (DC), and the onset of Australian monsoon. Chen et al. (2019c) summarized significant KW-synoptic event interactions in December 2016: two westward-propagating synoptic waves centered within 5 - 15°N led to KW enhancements, two synoptic disturbances were identified as pre-cursors of tropical depression/tropical cyclone, and the passage of a KW contributed to the Australian Summer Monsoon onset. They also found that the DC rainfall in MC was enhanced in major islands and neighboring oceans in the KW convec-

tive phase. The DC hotspots were modulated by background winds, the terrain effects over the islands, and the land-ocean geographic distribution in certain "coastal regime".

Following the same approach of Chen et al. (2019c), we show an analysis of December 2017. The monthly anomalies of SST, low-level wind, and rainfall for December 2017 are shown in Fig. 10. The figure shows warmer SST in western Pacific, a pair of cyclonic flow straddling western MC, and associated stronger rainfall in the two cyclonic centered over the southern SCS-Philippine Sea and eastern Indian Ocean south of Java. Figure 10 also shows much enhanced rainfall in equatorial western Pacific around 150°E where stronger trade winds from the east converged with anomalous westerly winds from the west. The above mentioned ocean-atmospheric coupled features bear a resemblance of anomalous SST-wind-rainfall for December 2016 (Chen et al. 2019c) and the composite fields of 9 La Niña years (Fig. 10c). However, we note that, in December 2017 (Figs. 10b, c), the anomalous low-level cyclonic center over the Philippines and the anomalous northeasterly winds over the SCS in phase with the winter monsoon all shifted westward in December 2016 with the anomalous cyclonic flow over the Indochina and anomalous southwesterly over the SCS against the background monsoon flow.

A quasi-stationary convection over the western Pacific near 150°E in the first half December 2017 as shown in the Hovmöller diagram of 5°S - 5°N averaged OLR (Fig. 11a) and the horizontal maps of OLR and 925-hPa streamline at every two days starting 6th December (Fig. 12). Since the quasi-stationary heating/westerly in western Pacific was preceded by anomalies of negative OLR and westerly wind over Indian Ocean during mid-November and early December 2017 (Fig. 8b), we regard it as a quasi-stationary ISO that is traced in Fig. 12 by the "ISO" mark in Day 6 - 16 maps. The ISO heating together with a stronger northeasterly monsoon background in the La Niña December (Fig. 10c) corresponded to a dry northern SCS but wet Philippine Sea in December 2017 (Fig. 13a). The anomalous dry northern SCS experienced several intruding northeasterly surges around 4 - 5, 8, 16, 24 of December 2017 as shown by the averaged northeasterlies along the Vietnam coast (Fig. 13b). The temporal evolution of vertical profiles of horizontal wind and relative humidity as shown by soundings at Dongsha (Fig. 14a) show clear drops of RH in the lower troposphere below 850 hPa corresponding to the surges of northeastlies. The soundings at Taping show similar drops in RH (Fig. 14b).

Combining Fig. 11a, the Hovmöller diagram of 5 - 15°N averaged OLR (Fig. 11b), and Fig. 12, we show that after December 11 the "ISO" in western Pacific coincided with an eastward propagating Kelvin Wave (KW1) around the equator and also with a westward propagating MT wave (MT1) off-equator in the NH. Heavy rainfall occurred in coastal area of Philippine Sea during 11 - 16 December (Fig. 13c). After 16 December, a major ER wave (ER1)
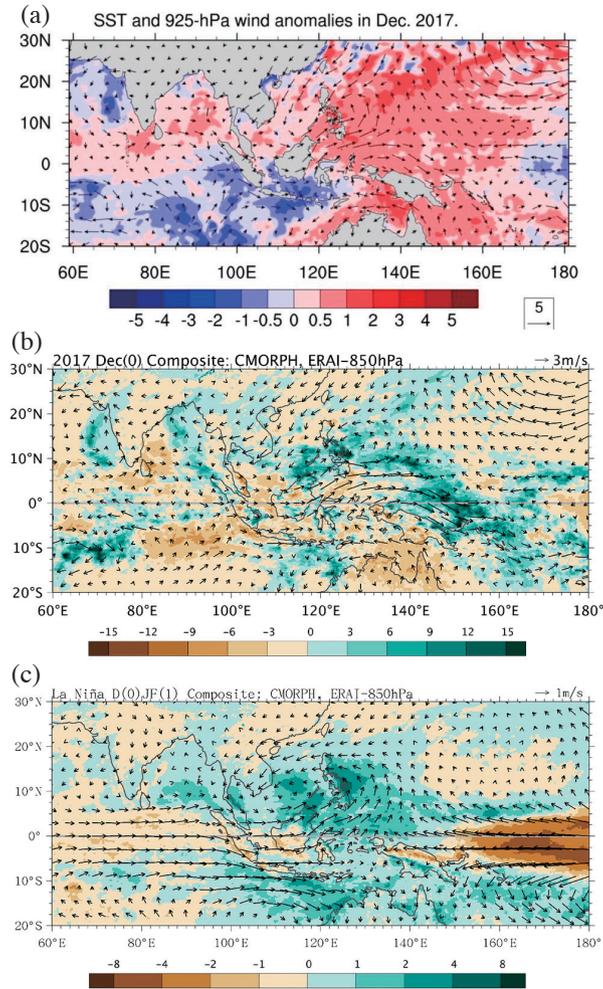
Fig. 10. (a) The NOAA OISST (shading; °C) and ERA-Interim 925-hPa wind (vectors; m s^{-1}) anomalies during December 2017. (b) The CMORPH precipitation (mm day^{-1}) and the ERA-Interim 850-hPa wind (vectors; m s^{-1}) anomalies for December 2017. (c) The CMORPH precipitation (shading; mm day^{-1}) and ERA-Interim 850-hPa wind (vectors) anomalies for La Niña composites. The anomalies are the deviation from the 1998 - 2016 monthly climatology. See Fig. 4 for the list of La Niña events.
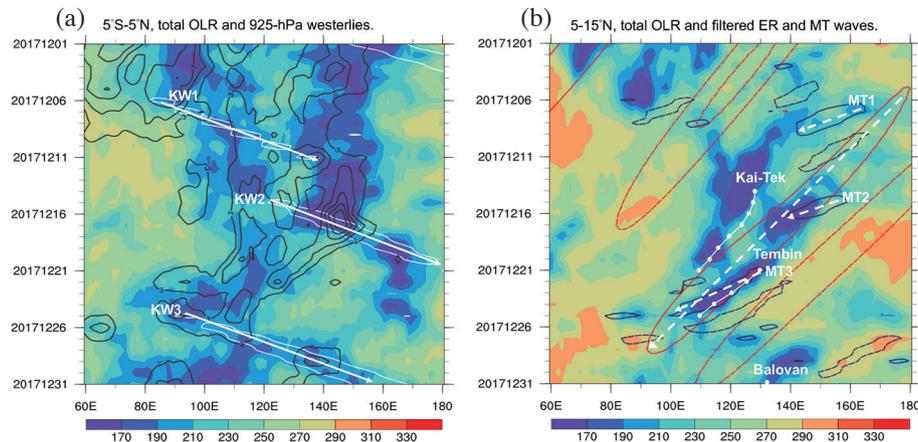

Fig. 11. (a) Hovmöller diagram in 5°S - 5°N latitudinal band of (a) total OLR (shading; W m^{-2}), 925-hPa westerly wind (black contour starts at 3 m s^{-1}, intervals at 2 m s^{-1}; only positive values are shown), and the filtered Kelvin waves (white contours, only convective phases in negative values are shown) in December 2017. White arrows show the propagation of the three KW events based on the filtered OLR contours. (b) Similar to (a) but for total OLR (shading), ER- (red contours) and MT- (dark blue contours) wave-filtered OLR within the 5 - 15°N latitudinal band; for ER and MT waves, the solid (dashed) contours are negative (positive) values at the interval of 10 and 15 W m^{-2}, respectively, and the zero-value contour is omitted. The white dashed arrows in (b) show the propagation of the ER and three MT events based on the filtered OLR contours. The white dots in (b) indicate the tracks of tropical cyclones, Kai-tek, Tembin, and Balovan.
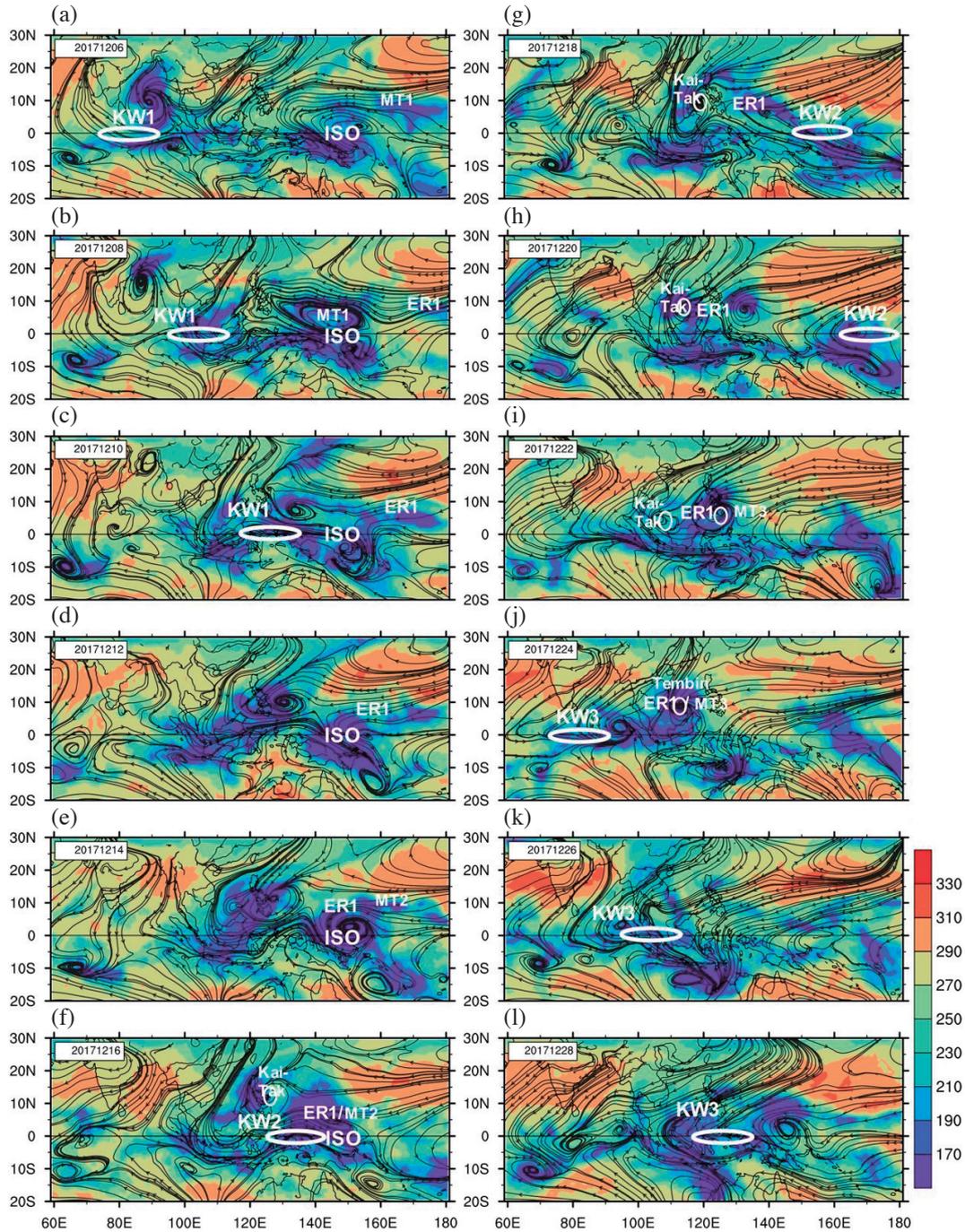
Fig. 12. Horizontal maps of OLR (shaded) and 925-hPa streamline for every two days from 6th to 28th in December 2017. The white ellipses represent KWs and small circles denote TC Kai-Tak, TC Tembin and MT3 based on the space-time filtered OLR signals. The ISO, ER, and MT waves are also labeled at their respective locations.
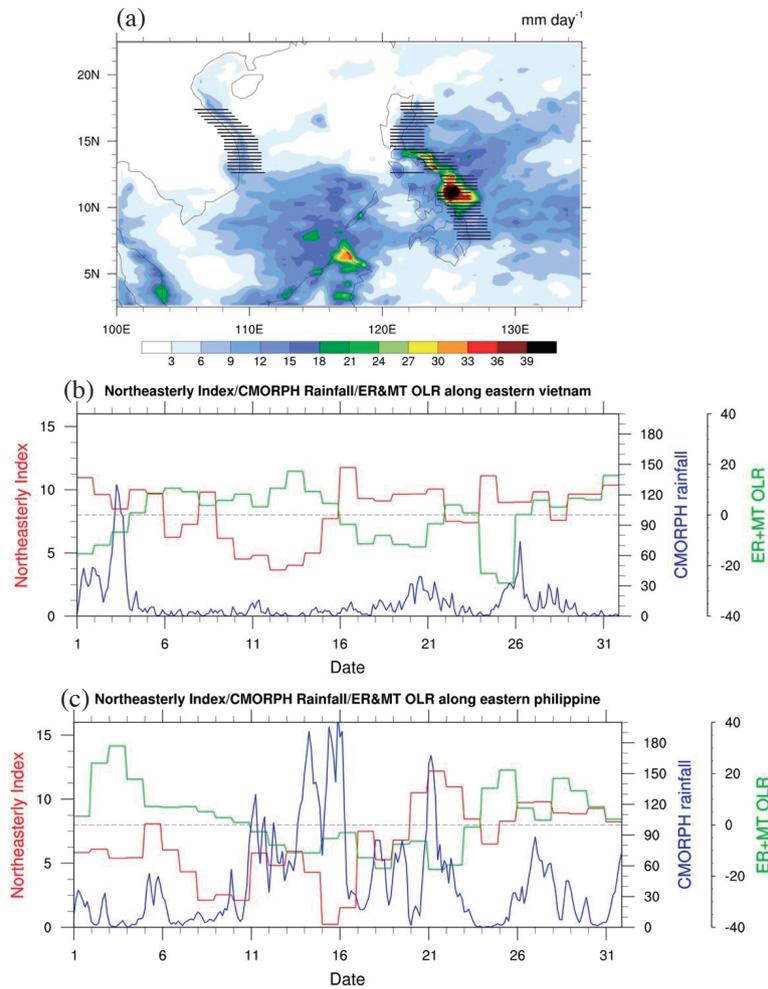
Fig. 13. (a) The monthly mean CMORPH rainfall (shading; mm day^{-1}) and the two monsoon windward regions along the eastern coast of Vietnam and Philippines consisting of grids marked by horizontal bars. (b) (c) The time series of the daily northeasterly index (m s^{-1}, red curve), the OLR anomaly (W m^{-2}, green curve) of ER and MRG/TD wave band, and 3 hourly CMORPH rainfall (mm day^{-1}, blue curve) over the eastern coast of Vietnam (b) and Philippine (c) defined in (a) during December 2017. Black horizontal dashed line indicates zero OLR anomaly of ER and MT waves.
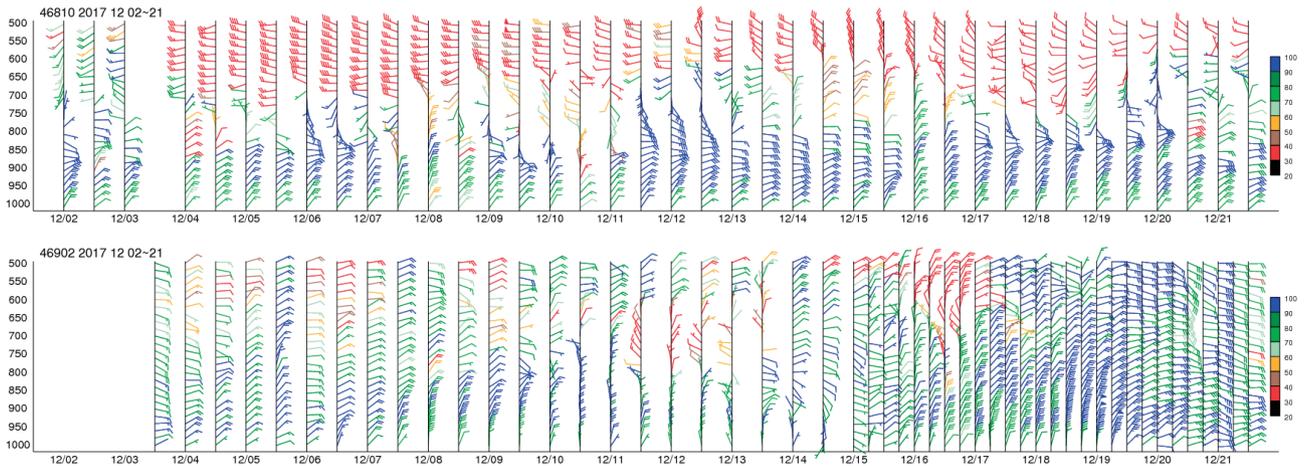

Fig. 14. Vertical and temporal distribution of horizontal winds (bar) and relative humidity (color) measured by radiosondes released at Donsha (upper) and Taiping (lower) during the IOP-W in December 2017.

and MT2 merged with the "ISO" near 140°E when a new Kelvin Wave (KW2) formed west of the ISO. Two named TCs, influencing the SCS during this month, namely Kai-Tak and Tembin, formed following the development of MT1 and MT3 in western Pacific near 13th and 24th. Kai-Tak reached the TS strength west of the Philippines near (127°E, 10°N) and moved into the SCS around 18th where strong northeasterly steered its path southwestward. Tembin formed near (134°E, 8°N) and moved into the SCS around 23rd and continued moving westward. They produced two rainfall peaks west of the Philippines near (123°E, 13°N) and (125°E, 11°N) shown in Fig. 13a, and the peaks near the coast of Philippines (Vietnam) around 15th and 21th (20th and 26th) December (Figs. 13b, c).

The influences of the ISO and CCEW on rainfall in the SCS and MC in December 2017 are summarized by a schematic figure by superimposing equatorial zonal wind with the CCEWs based on space-time filtered OLR in 5 - 15°N (Fig. 15). Two types of large-scale influences on rainfall in the SCS-MC region can be identified. One is the ISO, KW and associated ER and MT waves that cause much enhanced rainfall including heavy rainfall by the named TCs Kai-Tak and Tembin. This is similar to the dominant influence of a KW in December 2016 shown in Fig. 7 of Chen et al. (2019c) that a KW provided favorable conditions for the development of an ER, a MT, and later named TC Nock-ten that made landfall at the Philippines. The other type of large-scale influences on rainfall in the SCS-MC region involves the KW flow (equatorial westerly wind) approaching the west coast of Sumatra that led to enhanced convection west of Sumatra near 90°E as is evident in KW1 and KW3 in Fig. 15. The two KWs, however, appear to be weakened by topography of Sumatra where the zonal winds were interrupted/weakened but re-emerged near 110°E over southern SCS and Borneo where convection occurred likely due to cyclonic shear of the KW and enhanced diurnal heating (Baranowski et al. 2016a, b; Chen et al. 2019c). This type of interaction is also shown in Chen et al. (2019c).

Note that both December 2016 and December 2017 were in La Niña phase. Climatological analysis (Fig. 4b) indicates that eastern Indian Ocean to western MC is normally suppressed but eastern MC and western Pacific is convective in La Niña winters. Relative to the composite climatology, the evolution of December 2017 (Fig. 15) and December 2016 (Fig. 7 in Chen et al. 2019c) show weak wave activities in eastern Indian Ocean in December 2017 relative to that in December 2016. This is related to the strong Indian Ocean dipole signal in December 2017 as shown in Fig. 10.

Besides ISOs in the boreal winter seasons, we also analyzed intraseasonal variability in May 2018 that was in a decaying phase of La Niña (Lu et al. 2020). The study showed an eastward-moving ISO and westward-moving 10 - 20 day oscillation (or QBWO) in May 2018 that contributed to the delayed SCS monsoon onset in early June 2018.

Our analyses discussed in this section provide useful references for evaluations of model results of extended weather associated with intraseasonal oscillation (e.g., a study by Dr. Li-Hsuan Hsu and colleagues that is summarized in the following section, highlight 5). Such combined observational and modeling studies are required to improve the weather monitoring and forecast of this region.

6. PRELIMINARY SCIENTIFIC HIGHLIGHTS

We summarize in this section scientific highlights obtained so far from the SCSTIMX and related studies.

(1) Influences of Subseasonal Oscillations on the SCS summer monsoon onset in SCSTIMX-S (Lu et al. 2020)

The SCS monsoon onset (in earlier June) in 2018 was late relative to climatological seasonal transition (~ mid-May). The delay was attributed to an anomalous anticyclone extending from the SCS to Bay of Bengal that was partly maintained by an ISO heating over eastern IO and the Maritime Continent and partly by anomalous heating over northwestern Pacific due to La Niña induced circulation. A dry Rossby wave arrived at the SCS in late May further contributed to a late SCS monsoon onset.

(2) Modulation of the SCS-MC Subseasonal Peak rainfall by the MJO and CCEW in Boreal Winter (Tsai et al. 2020)

The modulation of subseasonal rainfall extreme (the highest 15-day accumulated rainfall during NDJF within 10° latitude × 10° longitude grids) by the MJO and CCEWs is analysed based on 20 years of CMORPH data (1998 - 2018). The primary influence of the MJO (MT and ER waves) is on the occurrence time (intensity) of the extreme events over oceanic (off-equatorial) areas. For the NDJF of 2016/17 and 2017/18 (SCSTIMX-W), the number of days contributed by the MJO and CCEWs to the extreme events is estimated. The MJO contributed more days of the extreme events over the SCS between 5 - 15°N in 2016/17 but over the equatorial SCS and MC between 5°N - 5°S in 2017/18. The ER waves also contributed more days of the extreme events along the 5 - 15°N belt over the SCS-MC region in both winters. This study will be applied to assess the subseasonal predictability of dynamical forecast models.

(3) Track variability of South China Sea-formed tropical cyclones modulated by seasonal and intraseasonal circulations (Chen et al. 2020)

TCs formed in the SCS tend to move in three preferred directions (N, NE, and W-NW). Seasonally, the dominant tracks are NE in May, from NE into W-NW in June, W-NW and N in July to September (JAS), and W-NW in October to November (ON). Formation of TCs with W-NW tracks is associated with a southeastward-extending monsoon trough and a northwestward-expanding western Pacific subtropical
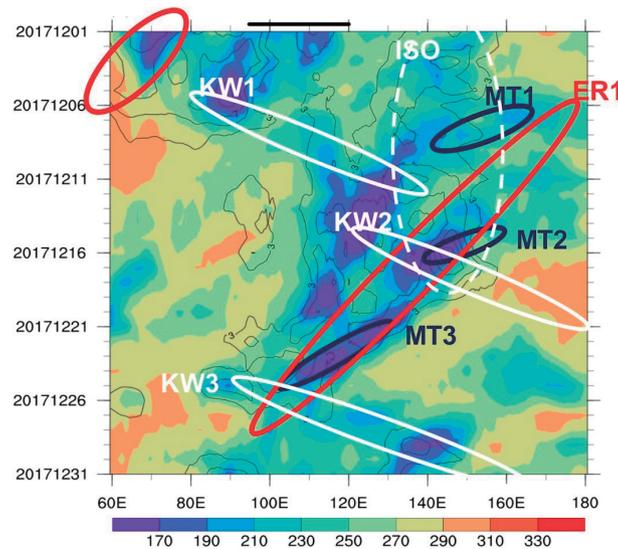
Fig. 15. A schematic figure explaining influences of ISO-CCEWs on rainfall in the SCS and MC in December 2017. The thin black contours are 925-hPa zonal wind in 5°S - 5°N, and the shading is the total OLR in 5 - 15°N. The smooth ellipses represent wave events based on the filtered OLR (white: KW, red: ER, black: MT). Named TC Kai-Tak and Tembin formed following the development of MT1 and MT3 near 13th and 24th over western Pacific and moved through Philippines into the SCS.

high (WPSH) in May to June (MJ), a southward-intensified monsoon trough and a westward-strengthened WPSH in JAS, and a northward and westward enhanced equatorial trough in ON. Formation of TCs with NE (N) tracks in MJ (JAS) is related to an eastward-intensified monsoon trough and an eastward-retreated (northwestward-extended) WPSH. For all track types, TCs tend to follow the propagation of the 10-24-day cyclonic anomaly to have different tracks. Their movement is assisted by favorable environments of moisture convergence provided by 30-60-day cyclonic anomalies distributing along TC tracks.

(4) Effects of convection-SST interactions on the South China Sea Summer Monsoon Onset in a Multiscale Modeling Framework Model (Kuo et al. 2020)

The effects of convection-SST interactions on the onset of the SCS Summer Monsoon was investigated by examining two simulations by the super-parameterized Community Atmosphere Model (SPCAM): CTRL with prescribed sea surface temperature climatology, and CPL with a coupled slab ocean model (SOM). The coupled simulation was shown to have improved boreal summer mean precipitation over Asia and the seasonal evolution in the SCS (like the mean pattern of synoptic flow and precipitation, the land-ocean diurnal cycle contrast during pre-onset stage). Since the coupling to SOM does not change the convection coupled physics in the SPCAM (like sensitivity of precipitation to column moisture), the improvements in CPL is partly attributed to the lower SST in response to air-sea interactions, and partly to the suppression of heavy precipitation under high SST regime likely associated with a different atmo-

spheric meridional circulation.

(5) A Simulation Study of Kelvin Waves Interacting with Synoptic Events During December 2016 in the South China Sea and the Maritime Continent (a submitted manuscript by Dr. Li-Hsuan Hsu and colleagues)

The Model for Prediction Across Scales (MPAS) was used to simulate the major events of scale interaction and associated dynamic-convective coupled structures in December 2016, with a fixed 60-km horizontal resolution and a variable 60-15-km resolution. Both versions of the model reasonably simulate the overall evolution of three KWs that interact with MT waves along with a winter monsoon cold surge, contributing to the formation of Cyclone Vardah, a strong Borneo vortex (BV), and Typhoon Nock-ten. With the 15-km grids covering SCS and western North Pacific, the simulation of the variable resolution model showed improved skills in the region, especially for the BV case. However, the MPAS 15-km resolution experiments have a tendency to produce more precipitation in the vicinity of TDs as well as in the convergence region associated with synoptic scale cold surges.

(6) The relationship between the boundary layer moisture transport from the South China Sea and heavy rainfall over Taiwan (Tu et al. 2020)

An analysis of heavy rainfall (> 80 mm day^{-1}) in June 2017 over Taiwan was performed using Climate Forecast System Reanalysis (CFSR) and rain gauge data. Three episodes of extreme rainfall occurred during 2 to 3 June (peak > 500 mm day^{-1}), 14 and 17 June (peaks > 300 mm day^{-1}).

These episodes were accompanied by large moisture transports within the marine boundary layer (MBL) from the northern SCS to Taiwan area. During 1 to 4 June and 14 to 18 June 2017, the integrated vapor transport [IVT] between surface and 900-hPa level exceeded 220 kg m^{-1} s^{-1} due to strong winds in the MBL (MBLJ). For both periods, the synoptic system-related low-level jet coexisted with the MBLJ. The MBLJ developed and intensified when the mei-yu trough over southern China deepened and/or the western Pacific subtropical high strengthened and extended westward. The moisture-laden MBLJs lifted by terrain and/or mei-yu jet/front systems produced heavy rainfall.

(7) Evolution of Water Budget and Precipitation Efficiency (PE) of Mesoscale Convective Systems (MCS) over the SCS (Wu et al. 2020)

The study focuses on the evolution of PE and water budget of MCSs formed within the humid southwesterly monsoon flow from Indo China in the SCS. Such an event during 25 to 28 August 2015 was investigated using the satellite observations and model simulations. Both semi-Lagrangian and Eulerian approaches were used to quantify the sensitivity of water budget and moisture fluxes to low-level moisture amount and wind speed. Results show that total condensation, deposition and surface precipitation (therefore PE) are highly sensitive to the low-level moisture changes due to resultant changes in moisture flux convergence within the MCS and changes in evaporation over the region of weak convection, like 10 - 20% decrease of moisture flux and 10 - 40% reduction of surface precipitation in response to 10% decrease of low-level (below 700 hPa) relative humidity.

7. RELEVANT SCSTIMX DATA AND WEB SITES

The SCSTIMX web page has been established to provide relevant information for the implementation of field campaigns, as well as the special observations obtained from the integrated project. The web pages contain 5 parts: Home, Weather Briefing, CWB WRF Model, PCCU YMC Plot Data, and Database Web Portal. "Home" includes contents such as a project introduction and progress reports. "Weather Briefing" contains summary reports of weekly meeting for real-time monitoring and prediction of S2S variability and weather events during the IOPs in 2017 and 2018. "CWB WRF Model" contains prediction outputs by a regional prediction model specifically developed by Central Weather Bureau for the SCSTIMX project (see a description below). The data contains 84-hr forecast of Taiwan and the South China Sea region made every day during May to October 2018. "PCCU YMC Plot Data" is observation data provided by Ching-Hwang Liu from PCCU during IOP-S, including surface observation data, skew-t graph, radar, and surface analysis, etc. "Database Web Portal" is the web interface of the SCSTIMX database which can be directly viewed and downloaded through the web browser. The database contains SCSTIMX observations described in section 2 and model output data for SCSTIMX described below. Generally, only the public files can be obtained through the Web portal. Unpublished files need to be logged in to obtain. The unpublished data will be available for download in the future.

7.1 The Central Weather Bureau (CWB) Regional Prediction Model

The Weather Research and Forecasting (WRF) based data assimilation system was implemented to configure the operational numerical weather prediction (NWP) system at Central Weather Bureau of Taiwan since 2007. The NWP system, so called CWB WRF, consists of the Advanced Research WRF dynamical core model (WRF-ARW; Skamarock et al. 2008), and the Hybrid 3DEnVAR data assimilation to take the advantage from the flow dependent background error covariance by the 32-member EAKF (Ensemble Adjustment Kalman Filter, Anderson 2001) data assimilation system. CWB WRF employs a partial cycling data assimilation scheme which begins with a cold start at 12 hr prior to the analysis time and cycling twice in every 6-hr interval (Hsiao et al. 2012). In addition, a blending method (Hsiao et al. 2015) is applied to merge the NCEP global analysis with the CWB WRF analysis using a spatial filter. The sophisticated data assimilation is so designed based on the following considerations: taking advantage of the global analysis, reducing the spin-up problem from the cyclic mesoscale data assimilation, and avoiding the accumulation of the model error, especially over the west Pacific area.

The nested model domains as shown in Fig. 16 were centered over Taiwan Island with horizontal resolution of 15-, and 3-km and 52 levels in the vertical. The outermost domain covered most of the Asian and west Pacific area in order to better describe the evolution of the subtropical high over the Pacific Ocean and to avoid the dilution from the lateral boundary problem due to the Tibetan Plateau. The model physics packages (Skamarock et al. 2008) include the Goddard microphysics scheme, the Kain-Fritch cumulus parameterization scheme, Yonsei University (YSU) planetary boundary layer scheme, NOAH land surface model, and the RRTMG longwave/shortwave radiation scheme. A standard Monin-Obukhov similarity theory was applied in the model surface layer to interpolate the wind field at 10-m AGL. CWB WRF was running 4 times a day, and provided hourly output up to 120-hr forecast length.

CWB WRF has been improved in various aspects including the model physics, initialization process, data assimilation and bug fixes. The synoptic scale verification, as shown in Fig. 17a, demonstrates a systematic improvement of the CWB WRF forecast skill from 2010 to 2018. A special edition of the operational system designed for typhoon prediction, so called TWRF, has the statistical typhoon track
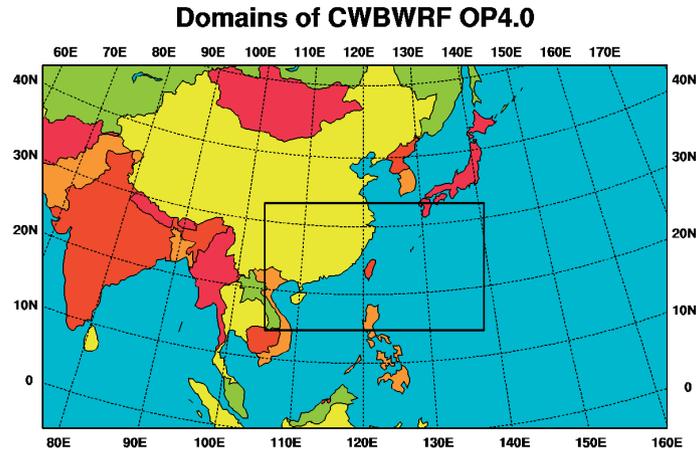
Domains of CWBWRF OP4.0

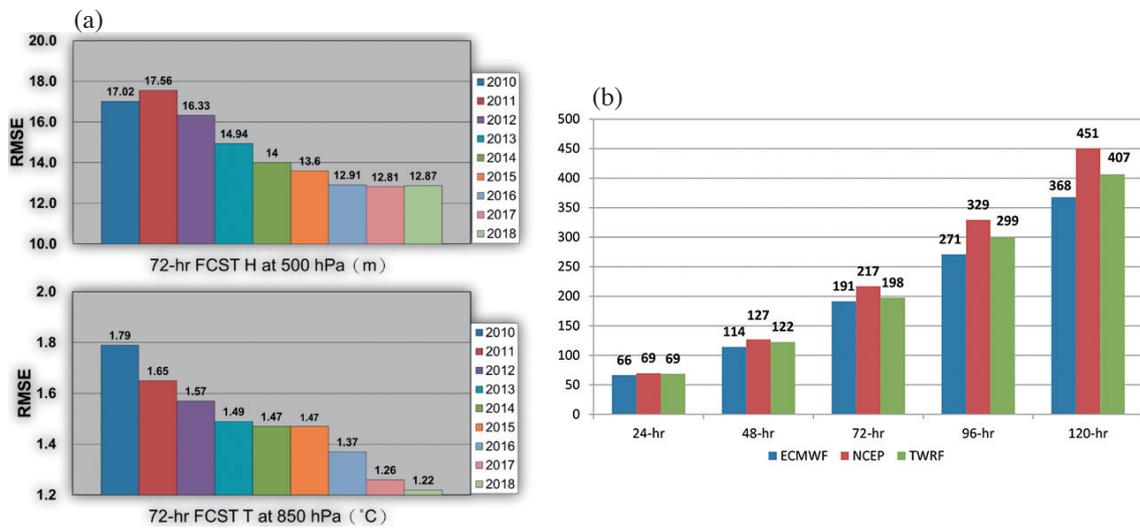Fig. 16. The domain coverage of CWB WRF model system.

Fig. 17. (a) The yearly averaged root mean square errors of 72-hr forecast for geopotential height at 500 hPa and temperature at 850 hPa of the outermost domain of the CWB WRF for the period of 2010 - 2018. (b) Averaged forecast errors of typhoon tracks over west Pacific area for ECMWF, NCEP, and TWRF for the three years of 2016 - 2018.

forecast error comparable to that in ECMWF and slightly better than NCEP GFS (Fig. 17b).

To provide more information about the daily weather during SCSTIMX period, CWB WRF was re-configured for the domains as shown in Fig. 18. The outer domain covers India, East Asia and whole Indonesia with 15-km horizontal resolution, and the inner domain covers the whole South China Sea region with a grid spacing of 3-km. The initial condition was provided by the cold start from the WRF 3DVAR, which assimilated observational data including SYNOP, SHIPS, METAR, PILOT, SOUND, SATEM, GPSRO, AIREP, and BUOY, etc. In this particular model system, the large domain of high resolution was designed to better resolve the multi-scale phenomena of the convection over the MC-SCS with large-scale flow during the SCSTIMX period.

7.2 The Taiwan Typhoon and Flood Research Institute (TTFRI) Global Prediction

TTFRI developed a global prediction system based on Model for Prediction Across Scales (MPAS). The system has been used for operational 10-day forecasts from 2015 to 2018. MPAS is a nonhydrostatic global atmospheric model with unstructured centroidal Voronoi mesh and C-grid staggering of the state variables (Skamarock et al. 2012). A variable resolution mesh is used for the operational forecast experiments (Fig. 19). The 15-km resolution area was centered at (20°N, 140°E) and covered the area of Western Pacific, Taiwan, Philippines, and the SCS, with a transition zone from 15 to 60 km in the surrounding boundary and 60-km resolution in the rest of the globe. Model is initialized with the NCEP GFS 00UTC analysis data every day. Model
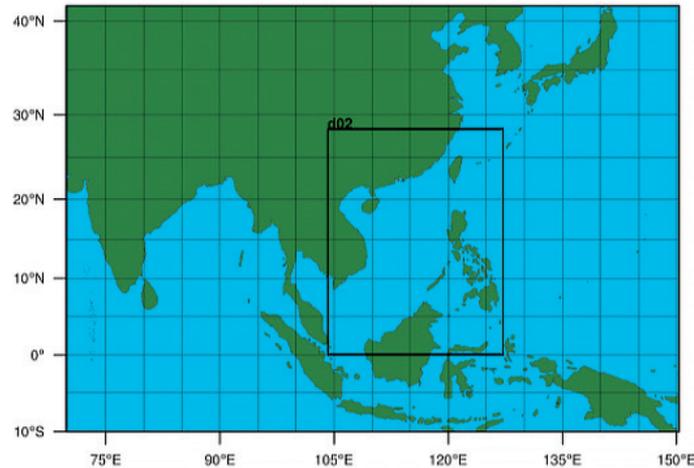
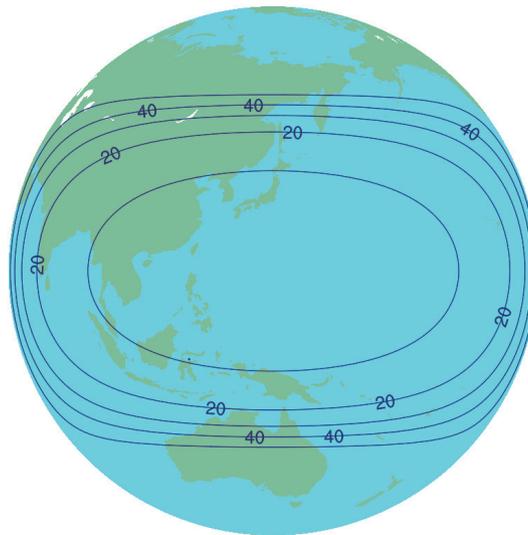Fig. 18. The domain of the WRF prediction model designed for the SCSTIMX.

Fig. 19. A variable-resolution mesh from the 15-km refinement area centered at (20°N, 140°E) through a transition domain of variable resolustion to a near-uniform 60 km cell spacing over the rest of the globe.

physics used in the experiments consist of the following:

(1) WRF Model Single-Moment 6-class microphysics (WSM6; Hong and Lim 2006);
(2) Tiedtke convective cumulus scheme (Zhang et al. 2011);
(3) Yonsei University (YSU) planetary boundary layer parameterization (Hong et al. 2006), Monin-Obukhov surface layer parameterization;
(4) Noah land surface model;
(5) Rapid Radiative Transfer Model for GCM applications (RRTMG) longwave and shortwave radiation parameterizations (Iacono et al. 2008).

The model performance is evaluated by comparing predicted low-frequency oscillations in Indo-Pacific warm pool and synoptic disturbances in the South China Sea and the Maritime Continent with the observed features in De-cember 2016. This is discussed in section 6 (5).

The Central Weather Bureau of Taiwan provided part of the computer resources.

REFERENCES

Adames, Á. F. and D. Kim, 2016: The MJO as a Dispersive, Convectively Coupled Moisture Wave: Theory and Observations. *J. Atmos. Sci.*, **73**, 913-941, doi: 10.1175/JAS-D-15-0170.1. [Link]

Adler, R. F., G. J. Huffman, A. Chang, R. Ferraro, P.-P. Xie, J. Janowiak, B. Rudolf, U. Schneider, S. Curtis, D. Bolvin, A. Gruber, J. Susskind, P. Arkin, and E. Nelkin, 2003: The Version-2 Global Precipitation Climatology Project (GPCP) Monthly Precipitation Analysis (1979-Present). *J. Hydrometeorol.*, **4**, 1147-1167, doi: 10.1175/1525-7541(2003)004<1147:TVGPCP>2.0. CO;2. [Link]

Ahn, M.-S., D. Kim, Y.-G. Ham, and S. Park, 2020: Role of Maritime Continent land convection on the mean state and MJO propagation. *J. Clim.*, **33**, 1659-1675, doi: 10.1175/jcli-d-19-0342.1. [Link]

Anderson, J. L., 2001: An ensemble adjustment Kalman filter for data assimilation. *Mon. Weather Rev.*, **129**, 2884-2903, doi: 10.1175/1520-0493(2001)129<2884:aeakff>2.0.co;2. [Link]

Annamalai, H. and J. M. Slingo, 2001: Active/break cycles: Diagnosis of the intraseasonal variability of the Asian Summer Monsoon. *Clim. Dyn.*, **18**, 85-102, doi: 10.1007/s003820100161. [Link]

Banzon, V., T. M. Smith, T. M. Chin, C. Liu, and W. Hankins, 2016: A long-term record of blended satellite and in situ sea-surface temperature for climate monitoring, modeling and environmental studies. *Earth Syst. Sci. Data*, **8**, 165-176, doi: 10.5194/essd-8-165-2016. [Link]

Baranowski, D. B., M. K. Flatau, P. J. Flatau, and A. J. Matthews, 2016a: Impact of atmospheric convectively coupled equatorial Kelvin waves on upper ocean variability. *J. Geophys. Res.*, **121**, 2045-2059, doi: 10.1002/2015JD024150. [Link]

Baranowski, D. B., M. K. Flatau, P. J. Flatau, and A. J. Matthews, 2016b: Phase locking between atmospheric convectively coupled equatorial Kelvin waves and the diurnal cycle of precipitation over the Maritime Continent. *Geophys. Res. Lett.*, **43**, 8269-8276, doi: 10.1002/2016GL069602. [Link]

Berrisford, P., D. Dee, P. Poli, R. Brugge, K. Fielding, M. Fuentes, P. Kållberg, S. Kobayashi, S. Uppala, and A. Simmons, 2011: The ERA-Interim Archive Version 2.0, ERA Report Series, ECMWF, Shinfield Park, Reading, 23 pp. Available at https://www.ecmwf.int/node/8174.

Chang, C.-P. and K. M. Lau, 1982: Short-Term Planetary-Scale Interactions over the Tropics and Midlatitudes during Northern Winter. Part I: Contrasts between Active and Inactive Periods. *Mon. Weather Rev.*, **110**, 933-946, doi: 10.1175/1520-0493(1982)110<0933:STPSIO>2.0.CO;2. [Link]

Chang, C.-P., Z. Wang, J. Ju, and T. Li, 2004: On the Relationship between Western Maritime Continent Monsoon Rainfall and ENSO during Northern Winter. *J. Clim.*, **17**, 665-672, doi: 10.1175/1520-0442(2004)017<0665:OTRBWM>2.0.CO;2. [Link]

Chang, C.-P., Z. Wang, J. McBride, and C.-H. Liu, 2005: Annual cycle of Southeast Asia—Maritime continent rainfall and the asymmetric monsoon transition. *J. Clim.*, **18**, 287-301, doi: 10.1175/JCLI-3257.1. [Link]

Chang, C.-P., M.-M. Lu, and H. Lim, 2016: Monsoon Convection in the Maritime Continent: Interaction of Large-Scale Motion and Complex Terrain. *Meteorol. Monogr.*, **56**, 6.1-6.29, doi: 10.1175/AMSMONOGRAPHS-D-15-0011.1. [Link]

Chang, C.-P., T. Li, and S. Yang, 2017: Monsoon rainfall prediction problem in the western Maritime Continent. In: Chang, C.-P. (Ed.), The Sixth WMO International Workshop on Monsoons (IWM-VI), Abstracts Volume, World Scientific Publishing Company, 155-160.

Chatterjee, P. and B. N. Goswami, 2004: Structure, genesis and scale selection of the tropical quasi-biweekly mode. *Q. J. R. Meteorol. Soc.*, **130**, 1171-1194, doi: 10.1256/qj.03.133. [Link]

Chen, G. and C.-H. Sui, 2010: Characteristics and origin of quasi-biweekly oscillation over the western North Pacific during boreal summer. *J. Geophys. Res.*, **115**, D14113, doi: 10.1029/2009JD013389. [Link]

Chen, J.-M., P.-H. Lin, C.-H. Wu, and C.-H. Sui, 2020: Track variability of South China Sea-formed tropical cyclones modulated by seasonal and intraseasonal circulations. *Terr. Atmos. Ocean. Sci.*, **31**, 239-259, doi: 10.3319/TAO.2019.11.07.02. [Link]

Chen, T.-C. and J.-M. Chen, 1995: An Observational Study of the South China Sea Monsoon during the 1979 Summer: Onset and Life Cycle. *Mon. Weather Rev.*, **123**, 2295-2318, doi: 10.1175/1520-0493(1995)123<2295:AOSOTS>2.0.CO;2. [Link]

Chen, T.-C. and M. Murakami, 1988: The 30-50 Day Variation of Convective Activity over the Western Pacific Ocean with Emphasis on the Northwestern Region. *Mon. Weather Rev.*, **116**, 892-906, doi: 10.1175/1520-0493(1988)116<0892:TDVOCA>2.0.CO;2. [Link]

Chen, W.-T., C.-M. Wu, W.-M. Tsai, P.-J. Chen, and P.-Y. Chen, 2019a: Role of coastal convection to moisture buildup during the South China Sea summer monsoon onset. *J. Meteorol. Soc. Jpn.*, **97**, 1155-1171, doi: 10.2151/jmsj.2019-065. [Link]

Chen, W.-T., C.-M. Wu, and H.-Y. Ma, 2019b: Evaluating the bias of South China Sea summer monsoon

precipitation associated with fast physical processes using a climate model hindcast approach. *J. Clim.*, **32**, 4491-4507, doi: 10.1175/JCLI-D-18-0660.1. [Link]

Chen, W.-T., S.-P. Hsu, Y.-H. Tsai, and C.-H. Sui, 2019c: The Influences of Convectively Coupled Kelvin Waves on Multiscale Rainfall Variability over the South China Sea and Maritime Continent in December 2016. *J. Clim.*, **32**, 6977-6993, doi: 10.1175/jcli-d-18-0471.1. [Link]

Chiang, J. C. H. and D. J. Vimont, 2004: Analogous Pacific and Atlantic meridional modes of tropical atmosphere-ocean variability. *J. Clim.*, **17**, 4143-4158, doi: 10.1175/JCLI4953.1. [Link]

DeMott, C. A., C. Stan, and D. A. Randall, 2013: Northward Propagation Mechanisms of the Boreal Summer Intraseasonal Oscillation in the ERA-Interim and SP-CCSM. *J. Clim.*, **26**, 1973-1992, doi: 10.1175/JCLI-D-12-00191.1. [Link]

Drbohlav, H.-K. L. and B. Wang, 2005: Mechanism of the Northward-Propagating Intraseasonal Oscillation: Insights from a Zonally Symmetric Model. *J. Clim.*, **18**, 952-972, doi: 10.1175/JCLI3306.1. [Link]

Fan, L., Q. Liu, C. Wang, and F. Guo, 2017: Indian Ocean dipole modes associated with different types of ENSO development. *J. Clim.*, **30**, 2233-2249, doi: 10.1175/JCLI-D-16-0426.1. [Link]

Feng, R. and W. Duan, 2018: The role of initial signals in the tropical Pacific Ocean in predictions of negative Indian Ocean dipole events. *Sci. China Earth Sci.*, **61**, 1832-1843, doi: 10.1007/s11430-018-9296-2. [Link]

Fukutomi, Y. and T. Yasunari, 1999: 10-25 day intraseasonal variations of convection and circulation over East Asia and western North Pacific during early summer. *J. Meteorol. Soc. Jpn.*, **77**, 753-769, doi: 10.2151/jmsj1965.77.3_753. [Link]

Goswami, P. and V. Mathew, 1994: A Mechanism of Scale Selection in Tropical Circulation at Observed Intraseasonal Frequencies. *J. Atmos. Sci.*, **51**, 3155-3166, doi: 10.1175/1520-0469(1994)051<3155:AMOSSI>2.0.CO;2. [Link]

Hamada, J.-I., M. D. Yamanaka, J. Matsumoto, S. Fukao, P. A. Winarso, and T. Sribimawati, 2002: Spatial and Temporal Variations of the Rainy Season over Indonesia and their Link to ENSO. *J. Meteorol. Soc. Jpn.*, **80**, 285-310, doi: 10.2151/jmsj.80.285. [Link]

Haylock, M. and J. McBride, 2001: Spatial Coherence and Predictability of Indonesian Wet Season Rainfall. *J. Clim.*, **14**, 3882-3887, doi: 10.1175/1520-0442(2001)014<3882:SCAPOI>2.0.CO;2. [Link]

He, H., J. W. McGinnis, Z. Song, and M. Yanai, 1987: Onset of the Asian Summer Monsoon in 1979 and the Effect of the Tibetan Plateau. *Mon. Weather Rev.*, **115**, 1966-1995, doi: 10.1175/1520-0493(1987)115<1966:OOT

ASM>2.0.CO;2. [Link]

He, J., H. Lin, and Z. Wu, 2011: Another look at influences of the Madden-Julian Oscillation on the wintertime East Asian weather. *J. Geophys. Res.*, **116**, D03109, doi: 10.1029/2010JD014787. [Link]

Hendon, H. H., 2003: Indonesian Rainfall Variability: Impacts of ENSO and Local Air-Sea Interaction. *J. Clim.*, **16**, 1775-1790, doi: 10.1175/1520-0442(2003)016<1775:IRVIOE>2.0.CO;2. [Link]

Hong, S.-Y. and J.-O. J. Lim, 2006: The WRF single-moment 6-class microphysics scheme (WSM6). *J. Korean Meteorol. Soc.*, **42**, 129-151.

Hong, S.-Y., Y. Noh, and J. Dudhia, 2006: A New Vertical Diffusion Package with an Explicit Treatment of Entrainment Processes. *Mon. Weather Rev.*, **134**, 2318-2341, doi: 10.1175/MWR3199.1. [Link]

Houze, R. A., S. G. Geotis, F. D. Marks, and A. K. West, 1981: Winter Monsoon Convection in the Vicinity of North Borneo. Part I: Structure and Time Variation of the Clouds and Precipitation. *Mon. Weather Rev.*, **109**, 1595-1614, doi: 10.1175/1520-0493(1981)109<1595:WMCITV>2.0.CO;2. [Link]

Hsiao, L.-F., D.-S. Chen, Y.-H. Kuo, Y.-R. Guo, T.-C. Yeh, J.-S. Hong, C.-T. Fong, and C.-S. Lee, 2012: Application of WRF 3DVAR to operational typhoon prediction in Taiwan: Impact of outer loop and partial cycling approaches. *Weather Forecast.*, **27**, 1249-1263, doi: 10.1175/waf-d-11-00131.1. [Link]

Hsiao, L.-F., X.-Y. Huang, Y.-H. Kuo, D.-S. Chen, H. Wang, C.-C. Tsai, T.-C. Yeh, J.-S. Hong, C.-T. Fong, and C.-S. Lee, 2015: Blending of Global and Regional Analyses with a Spatial Filter: Application to Typhoon Prediction over the Western North Pacific Ocean. *Weather Forecast.*, **30**, 754-770, doi: 10.1175/waf-d-14-00047.1. [Link]

Hsu, H.-H., 2005: East Asian monsoon. In: Lau, W. K. M. and D. E. Waliser (Eds.), Intraseasonal Variability in the Atmosphere-Ocean Climate System, Springer Praxis Books (Environmental Sciences), Springer, Berlin, Heidelberg, 63-94, doi: 10.1007/3-540-27250-X_3. [Link]

Hsu, H.-H. and C.-H. Weng, 2001: Northwestward Propagation of the Intraseasonal Oscillation in the Western North Pacific during the Boreal Summer: Structure and Mechanism. *J. Clim.*, **14**, 3834-3850, doi: 10.1175/1520-0442(2001)014<3834:NPOTIO>2.0.CO;2. [Link]

Huang, B., P. W. Thorne, V. F. Banzon, T. Boyer, G. Chepurin, J. H. Lawrimore, M. J. Menne, T. M. Smith, R. S. Vose, and H.-M. Zhang, 2017: NOAA Extended Reconstructed Sea Surface Temperature (ERSST), Version 5, NOAA National Centers for Environmental

Information, doi: 10.7289/V5T72FNM. [Link]

Hung, C.-S. and C.-H. Sui, 2018: A Diagnostic Study of the Evolution of the MJO from Indian Ocean to Maritime Continent: Wave Dynamics versus Advective Moistening Processes. *J. Clim.*, **31**, 4095-4115, doi: 10.1175/JCLI-D-17-0139.1. [Link]

Hung, C.-W., H.-J. Lin, and H.-H. Hsu, 2014: Madden-Julian Oscillation and the Winter Rainfall in Taiwan. *J. Clim.*, **27**, 4521-4530, doi: 10.1175/jcli-d-13-00435.1. [Link]

Iacono, M. J., J. S. Delamere, E. J. Mlawer, M. W. Shephard, S. A. Clough, and W. D. Collins, 2008: Radiative forcing by long-lived greenhouse gases: Calculations with the AER radiative transfer models. *J. Geophys. Res.*, **113**, D13103, doi: 10.1029/2008JD009944. [Link]

Izumo, T., M. Lengaigne, J. Vialard, J.-J. Luo, T. Yamagata, and G. Madec, 2014: Influence of Indian Ocean dipole and Pacific recharge on following year's El Niño: Interdecadal robustness. *Clim. Dyn.*, **42**, 291-310, doi: 10.1007/S00382-012-1628-1. [Link]

Jeong, J.-H., B.-M. Kim, C.-H. Ho, and Y.-H. Noh, 2008: Systematic variation in wintertime precipitation in East Asia by MJO-induced extratropical vertical motion. *J. Clim.*, **21**, 788-801, doi: 10.1175/2007JCLI1801.1. [Link]

Jiang, L. and T. Li, 2018: Why rainfall response to El Niño over Maritime Continent is weaker and non-uniform in boreal winter than in boreal summer. *Clim. Dyn.*, **51**, 1465-1483, doi: 10.1007/s00382-017-3965-6. [Link]

Jiang, X., T. Li, and B. Wang, 2004: Structures and Mechanisms of the Northward Propagating Boreal Summer Intraseasonal Oscillation. *J. Clim.*, **17**, 1022-1039, doi: 10.1175/1520-0442(2004)017<1022:SAMOTN>2.0.CO;2. [Link]

Joyce, R. J., J. E. Janowiak, P. A. Arkin, and P. Xie, 2004: CMORPH: A Method that Produces Global Precipitation Estimates from Passive Microwave and Infrared Data at High Spatial and Temporal Resolution. *J. Hydrometeorol.*, **5**, 487-503, doi: 10.1175/1525-7541(2004)005<0487:CAMTPG>2.0.CO;2. [Link]

Kalnay, E., M. Kanamitsu, R. Kistler, W. Collins, D. Deaven, L. Gandin, M. Iredell, S. Saha, G. White, J. Woollen, Y. Zhu, M. Chelliah, W. Ebisuzaki, W. Higgins, J. Janowiak, K. C. Mo, C. Ropelewski, J. Wang, A. Leetmaa, R. Reynolds, R. Jenne, and D. Joseph, 1996: The NCEP/NCAR 40-Year Reanalysis Project. *Bull. Amer. Meteorol. Soc.*, **77**, 437-472, doi: 10.1175/1520-0477(1996)077<0437:TNYRP>2.0.CO;2. [Link]

Kang, I.-S., C.-H. Ho, Y.-K. Lim, and K.-M. Lau, 1999: Principal Modes of Climatological Seasonal and Intraseasonal Variations of the Asian Summer Monsoon. *Mon. Weather Rev.*, **127**, 322-340, doi:

10.1175/1520-0493(1999)127<0322:PMOCSA>2.0.CO;2. [Link]

Kikuchi, K. and B. Wang, 2009: Global Perspective of the Quasi-Biweekly Oscillation. *J. Clim.*, **22**, 1340-1359, doi: 10.1175/2008JCLI2368.1. [Link]

Kikuchi, K., B. Wang, and Y. Kajikawa, 2012: Bimodal representation of the tropical intraseasonal oscillation. *Clim. Dyn.*, **38**, 1989-2000, doi: 10.1007/s00382-011-1159-1. [Link]

Krishnamurti, T. N. and P. Ardanuy, 1980: The 10 to 20-day westward propagating mode and "Breaks in the Monsoons". *Tellus*, **32**, 15-26, doi: 10.3402/tellusa.v32i1.10476. [Link]

Kug, J.-S., T. Li, S.-I. An, I.-S. Kang, J.-J. Luo, S. Masson, and T. Yamagata, 2006: Role of the ENSO–Indian Ocean coupling on ENSO variability in a coupled GCM. *Geophys. Res. Lett.*, **33**, L09710, doi: 10.1029/2005GL024916. [Link]

Kuo, K.-T., W.-T. Chen, and C.-M. Wu, 2020: Effects of convection-SST interactions on the South China Sea summer monsoon onset in a multiscale modeling framework model. *Terr. Atmos. Ocean. Sci.*, **31**, 211-225, doi: 10.3319/TAO.2019.08.16.01. [Link]

Lau, K.-M. and P. H. Chan, 1986: Aspects of the 40-50 Day Oscillation during the Northern Summer as Inferred from Outgoing Longwave Radiation. *Mon. Weather Rev.*, **114**, 1354-1367, doi: 10.1175/1520-0493(1986)114<1354:AOTDOD>2.0.CO;2. [Link]

Lau, K.-M. and C.-P. Chang, 1987: Planetary scale aspects of the winter monsoon and atmospheric teleconnections. In: Chang, C.-P. and T. N. Krishnamurti (Eds.), Monsoon Meteorology, Oxford Monographs on Geology and Geophysics, Oxford University Press, 161-202.

Lau, K.-M. and L. Peng, 1987: Origin of Low-Frequency (Intraseasonal) Oscillations in the Tropical Atmosphere. Part I: Basic Theory. *J. Atmos. Sci.*, **44**, 950-972, doi: 10.1175/1520-0469(1987)044<0950:OOLFOI>2.0.CO;2. [Link]

Lau, K.-M. and S. Yang, 1997: Climatology and interannual variability of the southeast asian summer monsoon. *Adv. Atmos. Sci.*, **14**, 141-162, doi: 10.1007/s00376-997-0016-y. [Link]

Lawrence, D. M. and P. J. Webster, 2002: The Boreal Summer Intraseasonal Oscillation: Relationship between Northward and Eastward Movement of Convection. *J. Atmos. Sci.*, **59**, 1593-1606, doi: 10.1175/1520-0469(2002)059<1593:TBSIOR>2.0.CO;2. [Link]

Lee, H.-T. and NOAA CDR Program, 2011: NOAA Climate Data Record (CDR) of Daily Outgoing Longwave Radiation (OLR), Version 1.2, NOAA National Climatic Data Center, doi: 10.7289/V5SJ1HH2. [Link]

Lee, J.-Y., B. Wang, M. C. Wheeler, X. Fu, D. E. Waliser, and I.-S. Kang, 2013: Real-time multivariate indices for the boreal summer intraseasonal oscillation over the Asian summer monsoon region. *Clim. Dyn.*, **40**, 493-509, doi: 10.1007/s00382-012-1544-4. [Link]

Li, T., B. Wang, C.-P. Chang, and Y. Zhang, 2003: A theory for the Indian Ocean dipole-zonal mode. *J. Atmos. Sci.*, **60**, 2119-2135, doi: 10.1175/1520-0469(2003)060<2119:ATFTIO>2.0.CO;2. [Link]

Lin, H. and B. Wang, 2002: The Time-Space Structure of the Asian-Pacific Summer Monsoon: A Fast Annual Cycle View. *J. Clim.*, **15**, 2001-2019, doi: 10.1175/1520-0442(2002)015<2001:TTSSOT>2.0.CO;2. [Link]

Ling, J., C. Zhang, R. Joyce, P. Xie, and G. Chen, 2019: Possible role of the diurnal cycle in land convection in the barrier effect on the MJO by the Maritime Continent. *Geophys. Res. Lett.*, **46**, 3001-3011, doi: 10.1029/2019GL081962. [Link]

Lu, M.-M., C.-H. Sui, J.-R. Sun, and P.-H. Lin, 2020: Influences of subseasonal to interannual oscillations on the SCS summer monsoon onset in 2018. *Terr. Atmos. Ocean. Sci.*, **31**, 197-209, doi: 10.3319/TAO.2020.02.25.01. [Link]

Luo, H. and M. Yanai, 1983: The Large-Scale Circulation and Heat Sources over the Tibetan Plateau and Surrounding Areas during the Early Summer of 1979. Part I: Precipitation and Kinematic Analyses. *Mon. Weather Rev.*, **111**, 922-944, doi: 10.1175/1520-0493(1983)111<0922:TLSCAH>2.0.CO;2. [Link]

Luo, J.-J., R. Zhang, S. K. Behera, Y. Masumoto, F.-F. Jin, R. Lukas, and T. Yamagata, 2010: Interaction between El Niño and extreme Indian Ocean dipole. *J. Clim.*, **23**, 726-742, doi: 10.1175/2009JCLI3104.1. [Link]

Madden, R. A. and P. R. Julian, 1972: Description of Global-Scale Circulation Cells in the Tropics with a 40-50 Day Period. *J. Atmos. Sci.*, **29**, 1109-1123, doi: 10.1175/1520-0469(1972)029<1109:DOGSCC>2.0.CO;2. [Link]

Maloney, E. D., 2009: The Moist Static Energy Budget of a Composite Tropical Intraseasonal Oscillation in a Climate Model. *J. Clim.*, **22**, 711-729, doi: 10.1175/2008JCLI2542.1. [Link]

Mao, J. and J. C. L. Chan, 2005: Intraseasonal Variability of the South China Sea Summer Monsoon. *J. Clim.*, **18**, 2388-2402, doi: 10.1175/JCLI3395.1. [Link]

Murakami, T., 1980a: Empirical Orthogonal Function Analysis of Satellite-Observed Outgoing Longwave Radiation During Summer. *Mon. Weather Rev.*, **108**, 205-222, doi: 10.1175/1520-0493(1980)108<0205:EOFAOS>2.0.CO;2. [Link]

Murakami, T., 1980b: Temporal Variations of Satellite-Observed Outgoing Longwave Radiation over the Winter Monsoon Region. Part I: Long-Period (15-30 Day) Oscillations. *Mon. Weather Rev.*, **108**, 408-426, doi: 10.1175/1520-0493(1980)108<0408:TVOSOO>2.0.CO;2. [Link]

Murakami, T. and J. Matsumoto, 1994: Summer monsoon over the Asian continent and western North Pacific. *J. Meteorol. Soc. Jpn.*, **72**, 719-745, doi: 10.2151/jmsj1965.72.5_719. [Link]

Nakazawa, T., 1992: Seasonal Phase Lock of Intraseasonal Variation during the Asian Summer Monsoon. *J. Meteorol. Soc. Jpn.*, **70**, 597-611, doi: 10.2151/jmsj1965.70.1b_597. [Link]

Neale, R. and J. Slingo, 2003: The Maritime Continent and Its Role in the Global Climate: A GCM Study. *J. Clim.*, **16**, 834-848, doi: 10.1175/1520-0442(2003)016<0834:TMCAIR>2.0.CO;2. [Link]

Nitta, T., 1987: Convective activities in the tropical western Pacific and their impact on the northern hemisphere summer circulation. *J. Meteorol. Soc. Jpn.*, **65**, 373-390, doi: 10.2151/jmsj1965.65.3_373. [Link]

Oh, J.-H., K.-Y. Kim, and G.-H. Lim, 2012: Impact of MJO on the diurnal cycle of rainfall over the western Maritime Continent in the austral summer. *Clim. Dyn.*, **38**, 1167-1180, doi: 10.1007/s00382-011-1237-4. [Link]

Oh, J.-H., B.-M. Kim, K.-Y. Kim, H.-J. Song, and G.-H. Lim, 2013: The impact of the diurnal cycle on the MJO over the Maritime Continent: A modeling study assimilating TRMM rain rate into global analysis. *Clim. Dyn.*, **40**, 893-911, doi: 10.1007/s00382-012-1419-8. [Link]

Peatman, S. C., A. J. Matthews, and D. P. Stevens, 2014: Propagation of the Madden-Julian Oscillation through the Maritime Continent and scale interaction with the diurnal cycle of precipitation. *Q. J. R. Meteorol. Soc.*, **140**, 814-825, doi: 10.1002/qj.2161. [Link]

Peatman, S. C., A. J. Matthews, and D. P. Stevens, 2015: Propagation of the Madden-Julian Oscillation and scale interaction with the diurnal cycle in a high-resolution GCM. *Clim. Dyn.*, **45**, 2901-2918, doi: 10.1007/s00382-015-2513-5. [Link]

Philander, S. G., 1990: El Niño, La Niña, and the Southern Oscillation, Volume 46, 1st Edition, Academic Press, 293 pp.

Qian, J.-H., 2008: Why precipitation is mostly concentrated over islands in the Maritime Continent. *J. Atmos. Sci.*, **65**, 1428-1441, doi: 10.1175/2007jas2422.1. [Link]

Ropelewski, C. F. and M. S. Halpert, 1987: Global and Regional Scale Precipitation Patterns Associated with the El Niño/Southern Oscillation. *Mon. Weather Rev.*, **115**, 1606-1626, doi: 10.1175/1520-0493(1987)115<1606:GARSPP>2.0.CO;2. [Link]

Saji, N. H., B. N. Goswami, P. N. Vinayachandran,

and T. Yamagata, 1999: A dipole mode in the tropical Indian Ocean. *Nature*, **401**, 360-363, doi: 10.1038/43854. [Link]

Sakaeda, N., G. Kiladis, and J. Dias, 2017: The Diurnal Cycle of Tropical Cloudiness and Rainfall Associated with the Madden-Julian Oscillation. *J. Clim.*, **30**, 3999-4020, doi: 10.1175/JCLI-D-16-0788.1. [Link]

Skamarock, W. C., J. B. Klemp, J. Dudhia, D. O. Gill, D. M. Barker, M. G. Duda, X.-Y. Huang, W. Wang, and J. G. Powers, 2008: A Description of the Advanced Research WRF Version 3, NCAR Technical Note, NCAR/TN-475+STR, University Corporation for Atmospheric Research, Boulder, Colorado, USA, doi: 10.5065/D68S4MVH. [Link]

Skamarock, W. C., J. B. Klemp, M. G. Duda, L. D. Fowler, S.-H. Park, and T. D. Ringler, 2012: A Multiscale Nonhydrostatic Atmospheric Model Using Centroidal Voronoi Tesselations and C-Grid Staggering. *Mon. Weather Rev.*, **140**, 3090-3105, doi: 10.1175/MWR-D-11-00215.1. [Link]

Sobel, A. and E. Maloney, 2012: An Idealized Semi-Empirical Framework for Modeling the Madden-Julian Oscillation. *J. Atmos. Sci.*, **69**, 1691-1705, doi: 10.1175/JAS-D-11-0118.1. [Link]

Sobel, A. and E. Maloney, 2013: Moisture Modes and the Eastward Propagation of the MJO. *J. Atmos. Sci.*, **70**, 187-192, doi: 10.1175/JAS-D-12-0189.1. [Link]

Tanaka, M., 1992: Intraseasonal Oscillation and the Onset and Retreat Dates of the Summer Monsoon over East, Southeast Asia and the Western Pacific Region using GMS High Cloud Amount Data. *J. Meteorol. Soc. Jpn.*, **70**, 613-629, doi: 10.2151/jmsj1965.70.1B_613. [Link]

Tao, S., L.-X. Chen, C.-P. Chang, and T. N. Krishnamurti, 1987: A review of recent research on the East Asian summer monsoon in China. In: Chang, C.-P. and T. N. Krishnamurti (Eds.), Monsoon Meteorology, Oxford Monographs on Geology and Geophysics, Oxford University Press, 60-92.

Tsai, W. Y.-H., M.-M. Lu, C.-H. Sui, and P.-H. Lin, 2020: MJO and CCEW modulation on South China Sea and Maritime Continent boreal winter subseasonal peak precipitation. *Terr. Atmos. Ocean. Sci.*, **31**, 177-195, doi: 10.3319/TAO.2019.10.28.01. [Link]

Tu, C.-C., Y.-L. Chen, P.-L. Lin, and P.-H. Lin, 2020: The relationship between the boundary layer moisture transport from the South China Sea and heavy rainfall over Taiwan. *Terr. Atmos. Ocean. Sci.*, **31**, 159-176, doi: 10.3319/TAO.2019.07.01.01. [Link]

Wang, B., 1994: On the Annual Cycle in the Tropical Eastern Central Pacific. *J. Clim.*, **7**, 1926-1942, doi: 10.1175/1520-0442(1994)007<1926:OTACIT>2.0.CO;2. [Link]

Wang, B. and G. Chen, 2017: A general theoretical frame-work for understanding essential dynamics of Madden-Julian oscillation. *Clim. Dyn.*, **49**, 2309-2328, doi: 10.1007/s00382-016-3448-1. [Link]

Wang, B. and T. Li, 1994: Convective Interaction with Boundary-Layer Dynamics in the Development of a Tropical Intraseasonal System. *J. Atmos. Sci.*, **51**, 1386-1400, doi: 10.1175/1520-0469(1994)051<1386:CIWBLD>2.0.CO;2. [Link]

Wang, B. and H. Lin, 2002: Rainy Season of the Asian-Pacific Summer Monsoon. *J. Clim.*, **15**, 386-398, doi: 10.1175/1520-0442(2002)015<0386:RSOTAP>2.0.CO;2. [Link]

Wang, B. and H. Rui, 1990: Dynamics of the Coupled Moist Kelvin-Rossby Wave on an Equatorial β-Plane. *J. Atmos. Sci.*, **47**, 397-413, doi: 10.1175/1520-0469(1990)047<0397:DOTCMK>2.0.CO;2. [Link]

Wang, B. and X. Xie, 1998: Coupled Modes of the Warm Pool Climate System. Part I: The Role of Air-Sea Interaction in Maintaining Madden-Julian Oscillation. *J. Clim.*, **11**, 2116-2135, doi: 10.1175/1520-0442-11.8.2116. [Link]

Wang, B. and X. Xu, 1997: Northern Hemisphere Summer Monsoon Singularities and Climatological Intraseasonal Oscillation. *J. Clim.*, **10**, 1071-1085, doi: 10.1175/1520-0442(1997)010<1071:NHSMSA>2.0.CO;2. [Link]

Wang, B., R. Wu, and X. Fu, 2000: Pacific-East Asian teleconnection: How does ENSO affect East Asian climate? *J. Clim.*, **13**, 1517-1536, doi: 10.1175/1520-0442(2000)013<1517:PEATHD>2.0.CO;2. [Link]

Wu, Y.-C., M.-J. Yang, and P.-H. Lin, 2020: Evolution of water budget and precipitation efficiency of mesoscale convective systems over the South China Sea. *Terr. Atmos. Ocean. Sci.*, **31**, 141-158, doi: 10.3319/TAO.2019.07.17.01. [Link]

Xie, P., R. Joyce, S. Wu, S.-H. Yoo, Y. Yarosh, F. Sun, and R. Lin, 2017: Reprocessed, Bias-Corrected CMORPH Global High-Resolution Precipitation Estimates from 1998. *J. Hydrometeorol.*, **18**, 1617-1641, doi: 10.1175/jhm-d-16-0168.1. [Link]

Xu, K., C. Zhu, and W. Wang, 2016: The cooperative impacts of the El Niño-Southern Oscillation and the Indian Ocean dipole on the interannual variability of autumn rainfall in China. *Int. J. Climatol.*, **36**, 1987-1999, doi: 10.1002/joc.4475. [Link]

Yamagata, T., S. K. Behera, J.-J. Luo, S. Masson, M. R. Jury, and S. A. Rao, 2004: Coupled ocean-atmosphere variability in the tropical Indian Ocean. In: Wang, C., S. P. Xie, and J. A. Carton (Eds.), Earth's Climate: The Ocean-Atmosphere Interaction, Volume 147, American Geophysical Union, 189-211, doi: 10.1029/147GM12. [Link]

Zhang, C., Y. Wang, and K. Hamilton, 2011: Improved Representation of Boundary Layer Clouds over the Southeast Pacific in ARW-WRF Using a Modified Tiedtke Cumulus Parameterization Scheme. *Mon. Weather Rev.*, **139**, 3489-3513, doi: 10.1175/MWR-D-10-05091.1. [Link]

Zhang, T., S. Yang, X. Jiang, and B. Huang, 2016a: Roles of Remote and Local Forcings in the Variation and Prediction of Regional Maritime Continent Rainfall in Wet and Dry Seasons. *J. Clim.*, **29**, 8871-8879, doi: 10.1175/JCLI-D-16-0417.1. [Link]

Zhang, T., S. Yang, X. Jiang, and P. Zhao, 2016b: Seasonal-Interannual Variation and Prediction of Wet and Dry Season Rainfall over the Maritime Continent: Roles of ENSO and Monsoon Circulation. *J. Clim.*, **29**, 3675-3695, doi: 10.1175/JCLI-D-15-0222.1. [Link]

Zhang, T., B. Huang, S. Yang, J. Chen, and X. Jiang, 2018: Dynamical and thermodynamical influences of the Maritime Continent on ENSO evolution. *Sci. Rep.*, **8**, doi: 10.1038/s41598-018-33436-5. [Link]